

1 **The joint sets on the Lilstock Benches, UK. Observations**
2 **based on mapping a full resolution UAV-based image**

3 **Martijn Passchier*¹, Cees W. Passchier², Christopher Weismüller³, Janos L. Urai¹**

4 ¹ Tectonics and Geodynamics, RWTH Aachen University, Lochnerstrasse 4-20, D-52056 Aachen, Germany,
5 www.ged.rwth-aachen.de; Urai – orcid 0000-0001-5299-6979

6 email: martijn.passchier@yahoo.de

7 email: j.urai@ged.rwth-aachen.de

8 ² Tektonophysik, Johannes Gutenberg University of Mainz, D-55099 Mainz, Germany. Orcid 0000-0002-3685-
9 7255

10 email: cpasschi@uni-mainz.de

11 ³ Neotectonics and Natural Hazards, RWTH Aachen University, Lochnerstrasse 4-20, D-52056 Aachen,
12 Germany, www.nug.rwth-aachen.de

13 email: c.weismueller@nug.rwth-aachen.de

14 *corresponding author: martijn.passchier@yahoo.de

15

16 This preprint was submitted to the Journal of Structural Geology for peer review.

17 **The joint sets on the Lilstock Benches, UK. Observations** 18 **based on mapping a full resolution UAV-based image**

19 **Martijn Passchier*¹, Cees W. Passchier², Christopher Weismüller³, Janos L. Urai¹**

20 ¹ Tectonics and Geodynamics, RWTH Aachen University, Lochnerstrasse 4-20, D-52056 Aachen, Germany,
21 www.ged.rwth-aachen.de; Urai – orcid 0000-0001-5299-6979

22 ² Tektonophysik, Johannes Gutenberg University of Mainz, D-55099 Mainz, Germany. Orcid 0000-0002-3685-
23 7255

24 ³ Neotectonics and Natural Hazards, RWTH Aachen University, Lochnerstrasse 4-20, D-52056 Aachen,
25 Germany, www.nug.rwth-aachen.de

26 *corresponding author: martijn.passchier@yahoo.de

27 **Keywords:** joint, Lilstock, joint abutment, UAV, fracturing

28 **Highlights**

- 29 • Full-resolution UAV-based image of the joint set of the classic Lilstock benches (UK)
- 30 • Layer-bound joints are fully imaged over an entire large outcrop
- 31 • Up to eight sets of joints occur in a single limestone layer
- 32 • Jointing is laterally heterogeneous in the same layer and different between layers
- 33 • Phases of sealing accompanied the evolution of older joints at Lilstock

34 **Abstract**

35 Outcrop studies of fracture networks are important to understand fractured reservoirs in the subsurface, but
36 complete maps of all fractures in large outcrops are rare due to limitations of outcrop and image resolution. We
37 manually mapped the first full-resolution UAV-based, Gigapixel dataset and DEM of the wave-cut Lilstock
38 Benches in the southern Bristol Channel basin, a classic outcrop of layer-bound fracture networks in limestones.
39 We present a map of the patterns and age relationships of successive sets of joints in dm-thick limestone layers
40 separated by claystone beds. Using interpretation criteria based on crosscutting relationships, abutting and joint
41 length, up to eight successive sets of joints were mapped. Results show that joint geometry and interrelations are
42 fully resolved in the whole outcrop. Different joint sets have unique characteristics in terms of shape, orientation,
43 spatial distribution and cross-cutting relations. The presence of low-angle crossings and junctions of joints
44 suggest periods of partial joint sealing and reactivation. The dataset and interpretations are proposed as an
45 outline for large scale, complete fracture network mapping to test digital fracture network models.

46 1. Introduction

47 Fractures in layered sedimentary rocks are amongst the most common and most intensely studied structures in
48 geology, present in nearly every outcrop (Pollard and Aydin, 1988; Price and Cosgrove, 1990; Twiss and
49 Moores 1992; Rawnsley et al., 1998, Belayneh, 2003, 2004; Peacock, 2004; Fossen 2016; Laubach et al., 2019).
50 Fracture networks form important reservoirs and pathways for mineralizing fluids, hydrocarbons and water in
51 sedimentary basins (Berkowitz, 2002; Bonnet et al., 2001; de Dreuzy et al., 2012; Olson et al., 2009; Tsang &
52 Neretnieks, 1998; Pyrak-Nolte & DePaolo, 2015), and their density, spacing, orientation and interrelation has
53 therefore been a common subject of study of structural geology (Dyer, 1988; Dershowitz and Herda, 1992;
54 Mandl, 2005; Peacock et al., 2018). To model fluid flow in fractured reservoirs, the 3D fracture network must be
55 predicted in volumes of rock, large enough to be representative. Such models should be based on reality, and
56 data are therefore needed on the geometry of natural fracture networks. Since most outcrops where fracture
57 networks can be observed are small, analysis of such networks has mostly been done by hand or on small photo
58 compilations for small volumes of rock (Belayneh and Cosgrove, 2004; Loosveld and Franssen, 1992). This is
59 useful, but in order to obtain realistic models, it should be tested whether such results still apply to the
60 arrangement of fractures in larger volumes of rock. For this purpose, large rock volumes, in the form of large
61 outcrops in well-exposed domains should be analysed. Unmanned aerial vehicle (UAV)-based photography has
62 recently started to provide data for such large-scale models (Pollyea & Fairley, 2011; Menegoni et al., 2018;
63 Wüstefeld et al., 2018).

64 The first aim of this study was to investigate if mapping of large outcrop surfaces with thousands of joints
65 contributes beyond the study of smaller scale domains. We demonstrate, using an example from the UK, that
66 such mapping, using UAVs, can indeed provide data that cannot be obtained from mapping small-scale outcrops.
67 Such large-scale studies can be applied in coastal outcrops, and well-exposed domains in mountain and desert
68 areas on Earth and is particularly promising in planetary science. A second aim of this paper is to investigate to
69 what extent fracture networks from large outcrop platforms can be subdivided into sets and generations, and if
70 traditional criteria of relative age and overprinting relations can be applied to fracture networks.

71 The Lilstock Benches in the British Channel in the UK ($51^{\circ}12.166'$ N, $003^{\circ}12.014'$ W; Fig. 1) are a classic
72 outcrop of faults and joint networks. The Benches are part of the Lilstock anticline, a large intertidal outcrop of
73 sub-horizontal layers of thin-bedded Jurassic limestone alternating with claystone layers. The limestone layers
74 contain a dense pattern of joints, augmented by weathering, that have been studied since 1990 (Loosveld and
75 Franssen, 1992) by several groups (section 1.2; e.g. Peacock and Sanderson, 1991; Dart et al., 1995; Rawnsley et
76 al., 1998; Peacock, 2004; Glen et al., 2005; Gillespie et al., 2011). Most studies were done on a small part of the
77 extensive coastal platforms or used data of low resolution (Fig. 1), and no attempt has been made to make a full
78 inventory of the complete joint network in the whole outcrop. One of the implicit assumptions in many such
79 studies is that a small outcrop will be representative for a larger domain. In this paper, building on first results of
80 Weismüller et al., 2020a, we show that this provides insufficient information to fully characterise the fracture
81 network, and oversimplifies the deformation history. We focussed this study on the Lilstock outcrop in order to
82 investigate how a joint pattern as at Lilstock can be mapped using a large UAV-based ortho-rectified
83 photomosaic, to (i) define criteria for determining the age relationship of the joints, and (ii) to provide a first

84 interpretation of the geometry and interference history of the entire joint network. The orthomosaic we compiled
85 covers a 350 x 700 m area of the Lilstock Benches with a pixel size of 7.5 mm, sufficient to resolve all joints for
86 the first time in a compilation of $4 \cdot 10^9$ pixels. The present paper is part of three publications using the dataset
87 (Weismüller et al., 2020a, b). Weismüller et al. (2020a) compares complete fracture maps from manual and
88 automatic tracing methods, analyses geometry and topology of the fracture networks and provides an
89 evolutionary model based on age relationships similar to the ones presented here. Weismüller et al., (2020b-open
90 access) presents the orthomosaic we used for joint interpretation to allow verification of our results. A shapefile
91 is also attached as supplementary material to the present paper. In a follow-up paper we will present a map
92 based on automated interpretation of all fractures.

93 *1.1. Terminology*

94 We use the terminology as follows (Pollard and Aydin, 1988; Price and Cosgrove 1990; Twiss and Moores
95 1992; Fossen 2016; Laubach et al., 2019): **fractures** are sharp planar discontinuities in otherwise massive rock;
96 **joints** are narrow opening-mode fractures (Laubach et al., 2019) with very small (less than one mm) or no
97 lateral displacement, while **faults** have displacement exceeding 1 mm parallel to the fracture. Cohesion along
98 fractures may be negligible or approach cohesion of the wall rock, depending on them by being (partly) sealed
99 by mineral growth in the fracture (Laubach et al., 2019). Sealing may occur at different stages in the
100 development of fractures after their initiation. We reserve the term **vein** to fractures sealed with a
101 macroscopically visible thickness of crystalline material different from the fabric of the adjacent rock. Joints
102 may be unsealed, without cohesion, or sealed by a minor amount of crystalline material providing cohesion
103 (Pollard and Aydin, 1988; Price and Cosgrove 1990; Twiss and Moores 1992; Fossen 2016; Laubach et al.,
104 2019). In our study, we mostly limit ourselves to joints. We did not make direct observations, to determine if
105 joints were sealed during part of their development, especially since sealing can be patchy or temporary: we have
106 not investigated the microstructure of joints but have restricted ourselves to the large-scale geometry of
107 macroscopically visible shape, orientation and intersection relations.

108 *1.2 Lilstock outcrop - geology*

109 The Bristol Channel Basin (West Somerset, UK) has experienced three main stages of deformation (Dart et al.,
110 1995). A first stage created east-west striking normal faults, followed by north-south directed compression that
111 led to partial inversion of the normal faults and folding. A third stage of NS compression resulted in NE-SW
112 striking sinistral strike-slip faults. Extension is thought to be lower Jurassic and Cretaceous in age, while
113 subsequent inversion and strike-slip deformation are interpreted to be Tertiary (Dart et al., 1995; Glen et al.,
114 2005). Burial was to a depth of about 1.5 km.

115 The Lilstock outcrops present weakly deformed Jurassic (blue Lias) sediments with large scale open folds,
116 faults, veins and joints formed during burial and uplift (Fig. 2b). Dm-scale limestone layers alternate with
117 claystone beds of more variable thickness, between 4 - 71cm. The thickness of the limestone and claystone
118 layers is laterally consistent. A single asymmetric E-W trending open anticline affects the entire Lilstock outcrop
119 with the hinge zone located directly south of the main fault (Fig. 1). The southern limb of the fold rapidly

120 steepens to the south while the northern limb of the anticline is less steep and outlines platforms of single
121 exposed horizontal layers known as “benches” (Fig. 1). The anticline is attributed to the second regional
122 deformation phase of north-south compression (Dart et al., 1995).

123 *1.3 Previous work on fractures in Lilstock*

124 Papers on the joints in Lilstock usually discuss small areas of this large outcrop. Key publications discuss the
125 relation of joints to faulting (Peacock and Sanderson, 1991; Rawnsley et al., 1998; Gillespie et al., 2011), vein
126 formation (Peacock, 2004) and basin inversion (Dart et al., 1995; Glen et al., 2005). The local joint pattern is
127 complex and formed in several sets due to overprinting generations of deformation (Dart et al., 1995). The
128 geometry of the joints has been extensively studied on selected parts of the outcrop (Gillespie et al., 2011;
129 Peacock, 2004). Some of the earliest work was by Loosveld and Franssen (1992) who used a helicopter to
130 photograph part of the outcrop and identified up to six sets of joints. This was followed by Rawnsley et al.,
131 (1998), who identified the well-known fans of first-set joints converging on asperities on faults. Engelder and
132 Peacock (2001) and Belayneh and Cosgrove (2004) interpreted five to six sets of joints, describing their
133 geometry and evolution. Figure 1 shows the approximate location of these studies, compared with the area
134 covered in this paper. Peacock (2001) showed that there is a temporal relation between joints, faults and veins in
135 the Lilstock outcrop (Peacock, 2004). Veins in Lilstock limestones have been studied by Caputo and Hancock
136 (1999) and Cosgrove (2001). Faults were the subject of numerous publications. This includes strike-slip faults
137 (Peacock and Sanderson, 1995; Willemse et al., 1997; Kelly et al., 1998), normal faults (Davison, 1995; Nemčok
138 and Gayer, 1996), their association with relays (Peacock and Sanderson, 1991, 1994) and normal fault inversion
139 (Brooks et al., 1988; Chadwick, 1993; Dart et al., 1995; Nemčok et al., 1995; Kelly et al., 1999). Stress models
140 inferred from the surface morphology of joints or aerial photographs have been studied by Belayneh (2004) and
141 Gillespie et al., (2011). Belayneh (2003) and Belayneh et al., (2006) performed fluid injection simulation studies
142 on the fracture network.

143 **2. Materials and Methods**

144 *2.1 UAV data acquisition*

145 The entire Lilstock outcrop was photographed at low tide on 19 - 20 June 2017. Since high tide covers the
146 outcrop, we started one day after neaps with a tidal range of 2.69m to 9.69m. The outcrop was surveyed on foot
147 after data acquisition by UAV to select key points for measurements and to take photographs with sub-
148 millimetric resolution. The UAV used was a Phantom 4 model by SZ DJI Technology Co., Ltd with a 12.4-
149 megapixel camera. Joints were photographed from an altitude of 20 – 25 m to obtain sufficient resolution to see
150 all joints present. Photos were merged into high-resolution digital orthomosaics using PhotoScan by Agisoft.
151 These images have a pixel size of 7.5 ± 1 mm (Fig. 2c). Ground truthing was done against sub-mm resolution
152 photographs of selected locations on the surface to validate our identification of all joints, which are enhanced in
153 visibility by wave erosion. Further details on the method used are published in Weismüller et al., (2020a) and the
154 original orthomosaic is available in Weismüller et al., (2020b) .

155 We extracted joint lengths and orientations for single joint traces using QGIS. Statistical values for joint lengths
156 in Table 2 were calculated using the NetworkGT plugin (Nyberg et al., 2018), which was also used to generate
157 the length weighted rose diagrams in Figure 6a. To further investigate the length distribution of joints within a
158 certain set, joint lengths were plotted as histograms in combination with their cumulative length distribution in
159 Figure 6b and as box and whisker plots in Figure 8.

160 To quantify the spacing between joints in a set, we used several scanlines oriented orthogonally to the mean joint
161 orientation of the respective set. The position of the scanline was chosen to overlap with an area where the
162 investigated array of joints is abundant, and the underlying base map of the fractured pavement is of good
163 quality. This allowed additional interpretations to provide a detailed estimation of the spacing between joints.
164 The position of additional interpretation of joints of the respective sets were marked along the scanlines. The
165 intersections of all interpreted joints along a scanline were then used to calculate the distance from the first joint
166 to the other joints along a scanline, as visualized in Figure 7. The distances between neighbouring joints
167 (intervals) were calculated and used to infer further statistical values, presented as spacing in Table 2 and
168 Figure 8.

169 The joints of set J1* are curved and therefore vary in orientation depending on the position along the trace where
170 its orientation is measured. The overall orientations of these curved joints were defined as the orientation along a
171 straight line from tip to tip. To further quantify the geometry of J1* joints, we calculated their curvature as the
172 quotient of the true length along the joints trace and the shortest distance between the tips. Curvature values of
173 single joints are plotted on a map as a colour gradient from white, for a curvature of 1 for a straight line, to red
174 for the relatively highest curvature value (Fig. 11). To investigate possible correlations between geometrical
175 attributes of J1* joints, orientation and lengths as well as orientation and curvature were plotted against each
176 other in Figure 12.

177 *2.2 Joint mapping criteria*

178 For this study, we mapped one complete Bench, part of layer IV in the local stratigraphy, to test to what extent
179 the sequence of joints can be analysed in a completely exposed layer, and if this sequence is laterally consistent
180 (Fig. 1). The exposed surface of this layer (named “Bench IV”) was naturally separated into two areas (W and E)
181 by an erosion gully and a thin strip of rock in which joints cannot be properly attributed (Fig. 1). The photo
182 mosaics were mapped in detail with a maximum resolution of 7.5 ± 1 mm and interpreted in terms of age
183 relations and overall shape. Images were manually interpreted using ArcGIS. Joints were traced as polygons
184 over their complete length. Joints were mapped and subdivided into sets using the following “traditional”
185 criteria:

- 186 (1) Joints that are straight or slightly curved but continuous despite crossing other joints, are interpreted
187 as one joint, of one set.
- 188 (2) Mapped joints are hierarchically assigned to specific relative age sets in relation to other sets of joints
189 by analysis of the intersections between joints. These intersections can either be of “X” shape
190 (crossing) or “T” shape (abutting) (Fig. 2a). Abutment is the main argument to assign relative ages to
191 the joints, while X-intersections do not provide such information. A secondary argument to assign

192 joints to a specific set is their length. In case of conflicting relations: force of number wins, provided
193 the conflict can be explained.

194 Attributes such as length and orientation were extracted from ArcGIS and plotted to illustrate basic statistics
195 (Figs. 6-8). Although we are able to image all fractures in the outcrop, we mapped only approximately every
196 second joint on the map. This procedure was the only way to process the data in a reasonable time and increased
197 the readability of the map, while not affecting overall results. The youngest joint set (J8) was only mapped in
198 one sub-area since it is different from other joints in the area, having a near random orientation and being so
199 closely spaced that it cannot be shown on the same scale as the older, longer joints.

200 **3. Results**

201 *3.1 Joint imaging*

202 The Lilstock outcrop is extraordinary, both in the number and density of exposed joints, and in the nature of their
203 weathering. Because of the local high tides, joints weather at the surface to a U-shape that allows imaging them
204 with the resolution of our images (Fig. 2b-e). This weathering pattern is observed for joints in every direction
205 while depth depends on the time period of exposure. Freshly exposed limestone layers show less weathering,
206 although joints are still visible on our images.

207 *3.2 Joints - Results of digital outcrop interpretation*

208 *3.2.1 Area W*

209 The Western Area (Area W) of Bench IV (Figs. 1, S1) contains eight sets of joints, some of which are only
210 present in part of this area (Fig. 3). The joint sets were dated with respect to each other using the criteria
211 described above. In the westernmost part of Area W, five sets of joints were recognized (Figs. 4c, 5; Table 1).
212 The first set (J1) has long joints that cross the entire Area W with a NW-SE trend and even continue into layers
213 II and III to the north (Figs. 3, 6). They are mostly between 7 and 22 m long but can reach up to 55 metres (Figs.
214 6, 8). In the westernmost part of Area W, the joints are abutted by a second set, J2, at a low angle to J1 (Fig. 4a).
215 J2 joints have the same length distribution as J1 joints (Figs. 6, 8) but are more closely spaced (Figs. 7, 8) and
216 mostly straight, bending only close to their termination against J1 joints to end in a T-shaped abutment (Fig. 4a).
217 Some J2 joints impinge upon other J2 joints. The angle between J1 and J2 joints decreases eastwards by a
218 change in orientation of the J1 joints, while J2 retains its orientation, till both sets of joints are subparallel. In the
219 centre of Area W, J1 and J2 joints can no longer be distinguished and are all mapped as J1 joints. Both sets of
220 joints disappear towards the east of Area W (Fig. 3).

221 NE-SW trending J3 joints are short and closely spaced joints although their spacing can vary (Figs. 4c, 7,8).
222 They are mostly less than 5 m in length (Figs. 6, 8). J3 joints occur over most of area W but disappear towards
223 the NE (Fig. 5). J4 joints make a small angle with J3 joints and are even shorter than these joints, usually less

224 than 3 m long (Figs. 5-8). They differ from J3 joints in being much further spaced apart (Figs. 7,8). J4 sets are
225 present throughout Area W (Figs. 3, 4d).

226 Three younger sets of joints, J5-J7, occur exclusively in the NE part of Area W (Figs. 4d, 5). J5 joints are
227 subparallel to J4 joints of this area (Table 1; Fig. 6) but locally impinge on J4 joints with a T-junction, proving
228 their relative age. J5 joints can be further distinguished from J4 joints by their greater length and spacing (Figs.
229 6-8), which is consistent throughout Area W, and their slightly curved geometry. J4 joints tend to be perfectly
230 straight, similar to J3 and J2 joints (Fig. 4d). J6 joints trend NW-SE and are strongly curved in contrast to older
231 sets (Fig. 4d,e). They impinge on J4 and J5 joints with a T-junction confirming their relative age. They are
232 shorter and less widely spaced than J5 joints, resembling J4 joints in that aspect (Figs. 6-8). J7 joints are also
233 curved, trend approximately NNW-SSE and abut all previous sets in T-shapes in locations where J5 and J6 joints
234 intersect (Figs. 3, 4d,e). They are very short with relatively narrow spacing (Figs. 6-8). Length weighted rose
235 plots (Fig. 6) show that J1-J5 joints have little variation in orientation of less than ca. 20° within each set and
236 show an anticlockwise change in orientation from NW-SE for J1 to SW-NE for J5 (Figs. 3, 5, 6). J6 and J7 joints
237 have quite different orientations (Fig. 6) and tend to be more curved than earlier sets. J7 varies considerably in
238 orientation over its range (Figs. 4d,e; 6, 8).

239 The youngest joints (J8) are very different from all previous joints (Fig. 4f). They have variable orientation,
240 abutting against all older joints and never crossing them (Figs. 4f, S2). The density of J8 joints varies between
241 stratigraphic layers of different thickness, creating different sized limestone blocks. However, block size also
242 depends on the density of older set joints. Stratigraphic layer IV (Bench IV) is twice as thick as layer III (Fig. 1),
243 but the limestone blocks delimited by J8 joints in Bench IV are smaller than in the adjacent layer, while the
244 opposite would be expected. This could be due to the density of older joints that is much higher in layer IV than
245 in the stratigraphic layers above, creating smaller blocks.

246 3.2.2 Area E

247 The eastern part of the investigated Bench IV, Area E, comprises a large exposed bench of the same layer IV as
248 in Area W, separated from it by a gully and a domain where joint sets cannot easily be attributed. (Figs. 5, 9;
249 Table 1). Labelling in Area E of the bench follows that of Area W, where more sets are present, with the addition
250 of an asterisk: joint sets recognised in Area E are labelled J1*, J4*, J5*, J6* and J8*. Because of their
251 orientation, separation and geometry, they are thought to correspond to joints with the same number in area W.

252 J1* joints occur locally and show pronounced fanning, converging on a fault (Gillespie et al., 2011) and thin out
253 towards the centre of the area (Figs. 5,9). The same relation can be found, with smaller fans of J1*, in other
254 stratigraphic layers, always related to the main fault (Figs. 5, S1). Single J1* joints cross most of the Bench in a
255 SE-NW direction. Shorter joints can be observed to abut joints of the same set, continuing in the same direction.
256 Besides a main fan in the SE, two smaller fans of J1* joints are visible on Bench IV as well (Figs. 5, 9). In the
257 westernmost part of Area E, the J1* joints have a trend of 140-150° and T-junctions show them to be older
258 than J4*.

259 J4* joints strike in the same direction and show the same characteristics of orientation, curvature, shape, length
260 and spacing as J4 joints of Area W, being the only example of joints that are easy to correlate over the entire
261 Bench IV (Figs. 5-9). J4* occurs throughout Area E, while other sets occur in a patchy manner.

262 J5*- and J6* joints are spatially separated, with only a small area of overlap where they show their relative age
263 through abutment (Figs. 5, 9). J5* is restricted to the western part of Area E but seem to cross into stratigraphic
264 layer III north of Area E (Figs. 5, 9). J6* and J4* joints abut each other in T-intersections with equal frequency
265 (Fig. 10a). This would seem to contradict the described method of age determination through T-intersections.
266 However, since J4* joints are clearly and consistently abutted by J5* joints, and these J5* joints in turn are
267 abutted by J6* joints, the age relation can be indirectly determined (Fig. 10b). J5* joints are considerably shorter
268 than J5 joints in Area W. They trend NE-SW but are slightly curved and show a considerable variation in
269 orientation due to fanning (Figs. 6, 8, 9). J6* joints trend NW-SE and are similar to J6 joints in length and
270 orientation. The youngest set (J8*) in Area E is similar to J8 in Area W, occurring perpendicular to older joints.
271 However, Area E presents domains of approximately 10 x 10 m with only few J4* and many J8* joints, resulting
272 in joint networks made up of nearly only J8* (Fig. 5c)

273 The transitional domain of Bench IV between areas W and E contains numerous joints in various directions, but
274 impingement relations are not clear since older joints cannot be followed for a long distance in the narrow Bench
275 (Figs. 1, 5). The reason is probably that joints of different sets happen to lie at a small angle with each other, and
276 older joints may have been reactivated to impinge on younger joints. This makes age relations unclear. In Areas
277 W and E, intermediate sets of joints occur which allow distinction of joint sets.

278 Outside Bench IV, joint set sequences and orientation may deviate from those in Bench IV, but relations have
279 not yet been mapped. For example, in layers south of Area W, the locally oldest set of joints follows the same
280 orientation as the hinge line of the main fold (Fig. 5). This parallelism to the hinge of the fold appears over a
281 large area and across multiple stratigraphic layers. Different stratigraphic layers seem to have different sets of
282 joints. While most layers have 2-3 sets, Bench IV shows up to 8 sets of joints with a maximum of approximately
283 six sets being present on 10m scale surfaces (Fig. 5c).

284 *3.2.3 Joint length*

285 Statistics of the mapped joint lengths for the entire Bench IV are shown in Table 2. The presented results should
286 be considered a first order estimate that might differ from the output of a complete interpretation of the entire
287 outcrop or complete interpretations within predefined domains. Therefore, it is important to view the presented
288 results as entirety and to less emphasize single attributes. Minimum length values for all sets are conservative
289 because of censoring of the traces and the tracing method.

290 Initial results show that sets J1, J2 and J5 are the groups with the overall longest joints of which J1 includes the
291 overall longest joints and J7 the shortest in Area W (Table 2; Figs. 6, 8). In Area E, the longest joints are in set
292 J1*. The calculated skewness is positive for all sets, indicating that the joint length distributions (Fig. 6) are
293 asymmetric with tails towards the right (longer fractures). This can also be observed in the histogram plots in
294 combination with the cumulative length distribution that show that most fractures within a set are small

295 (respectively within the set) and the respectively larger fractures are fewer, if not outliers, suggesting a typical
296 power-law distribution of the joints in all sets (Fig. 6). The kurtosis (Table 2) also describes the shape of the
297 length distribution. The small values for J1, J2, J4, J7, J4* and J6* indicate that the lengths are distributed close
298 to the mean length of the set, while the higher values of J3, J5, J6, J1* and J5* suggest distributions with a
299 stronger peak around the mean.

300 *3.2.4. Joint separation and curvature*

301 The intersections of joints within a certain set with a scanline are plotted in Fig. 7. Depending on the abundance
302 of the interpretation and the fractures in the dataset, the scanlines differ in length. However, the distribution of
303 the intersection along the scanline reveals slightly different patterns that consist of

- 304 i) evenly spaced joints over a distance along the scanline (e.g. J1_1 or J3_1),
- 305 ii) cases where joints are evenly distributed over shorter distances or sections along the scanline, but
306 less evenly over the entire length of the scanline (e.g. J1_2, J2_2, J3_3) because of “breaks” where
307 no joints intersect, or
- 308 iii) patterns that show sections with joints divided by breaks without joints, and different frequencies
309 of the joints within the sections where they are present (e.g. J7_1).

310 In some sets, joints are either fanning as set (J1*, J5*), or change orientation gradually (J1*, J5, J7; Figs. 3, 4, 6,
311 8, 9). The curvature of J1* joints is the most pronounced, as shown in Figure 11. Joints with higher curvature are
312 located at the margins of the fan structure where joints have a higher curvature than the ones in the center of the
313 structure. A plot of the orientation vs length of single J1* joints (Fig. 12a) reveals no clear relation of the two
314 values, as orientations spread over an interval of 100° with similar lengths, what is also the suggest by the rose
315 diagram in Figure 6. Also, the plot of curvature vs. orientation of the joints (Fig. 12b) does not reveal a clear
316 relationship of the two attributes.

317 **4. Discussion**

318 This study presents a manually interpreted map of joints in the famous Lilstock Benches, based on a complete
319 high-resolution digital image of the outcrop. Previous work has either used stitched photos of parts of the
320 outcrop, or images without the resolution to resolve all joints. Preparing the image was possible because the
321 joints are augmented by wave erosion, which allowed imaging all joints in this large outcrop with a UAV in one
322 single day. Comparison with close-up photos of selected sites with much higher resolution validates that the
323 resolution chosen is indeed sufficient: all joints are visible on our image (Weismüller et al., 2020). Our
324 observations are generally in agreement with existing studies, which have shown that the joints are younger than
325 the faults and veins in the outcrop, and developed during uplift, with stress concentrations at fault asperities
326 during the development of the first joint set, causing the well-known joint fans also present in other outcrops
327 around the Bristol channel (Bourne and Willemse, 2001; Maerten et al., 2018). However, our approach of

328 mapping the entire outcrop enhances the information that can be drawn from the observed joints, as outlined
329 below.

330 *4.1 Robustness of interpretation*

331 In agreement with earlier studies, we found that, since younger joints do not deform or displace older joints,
332 mapping of joint sets and distinguishing different sets is generally possible based on a few simple criteria
333 (Peacock et al., 2018):

- 334 1. assigning joints to a specific set is by orientation, abutment relations and length: the longest joints are
335 generally oldest.
- 336 2. joint intersections can be either of “X” or “T” shape (X and Y in Laubach et al., 2019). T-shaped
337 geometries are the main argument to assign relative ages to the joints.
- 338 3. joints that are straight or slightly curved but continuous despite cross-cutting other joints in X-
339 intersections, are interpreted as one joint.

340 Using these simple criteria, we could identify 8 age sets of joints over Bench IV, more than in any earlier study
341 (Fig. 8). However, in a number of cases analysis based on these criteria gives problematic results, as discussed
342 below. To check the robustness of the interpretations, selected areas were digitally mapped by a second
343 interpreter using the same criteria, with very similar results. In Table 1 we compare the different joint sets
344 interpreted in previous studies with the sets found in this project, as far as possible. The locations of the studied
345 joints of previous publications are shown in Figure 1. Sets of joints presented in the literature but missing in this
346 paper can be explained because these studies were done on a different bench. Although it is possible to recognise
347 sets of joints, the nature of the structure imposes inherent problems that are outlined below.

348 *4.2 Sample size and number of joint sets*

349 Our study shows that it is not possible to fully understand the full joint set content of the Lilstock Benches by
350 study of any small representative area. We can give a more complete and more complex image of the structural
351 content of one specific layer in the stratigraphy because of the larger extent of our database, Bench IV, compared
352 to earlier studies. First analysis of the joint sets present in Bench IV show that although at least eight sets of
353 joints are present over the entire Bench, several sets are always missing in smaller parts of the outcrop (Fig. 5).
354 Figure 5b shows the approximate boundaries of domains where different numbers of joints would be found in
355 small sample areas of 25 m². A small domain in the centre of Area W (about 2% of the Bench) has six sets of
356 joints that can be identified and relatively dated by abutting relations, while five sets can be found in four
357 subareas of Areas W and E (about 30% of the Bench), although each of these has a different group of joints.
358 Different groups of joints are also found in subdomains with fewer joint sets (Figs. 3, 5, 9). A smaller sample
359 domain than 25m² would show even fewer sets, and fewer abutting relations, so that relations of different sets
360 would remain uncertain. Small outcrops can therefore never reveal the complete picture, although set J4 can
361 form a bridge between subsamples in Bench IV.

362 4.3. Representativeness for joints in the subsurface

363 Since joints have been observed at the surface, subject to strong weathering, the question is to what extent they
364 are representative for joints found at depth, which have never been brought to the surface. In the worst case, the
365 joints we observe would be near-surface generated structures without any significance for subsurface structures.
366 The presence of up to eight subsequent generations of joints, each with its characteristic orientation, length and
367 inter-distance relations, however, makes it unlikely that these all formed at or near the surface. The only joints
368 that are most likely near-surface related or formed during uplift are the youngest generation J8/J8*. These joints
369 are the most numerous, in terms of total length of joints per m², abut against older joints, and do not cross these,
370 probably because these youngest joints formed during uplift when older joints had opened (Figs. 4f, S2). J8/J8*
371 joints have highly variable orientation. This indicates that these joints formed in the remaining unjointed islands
372 until the layer was saturated, their orientation controlled by the surrounding older joints of different sets.

373 4.4 Properties of the observed joint sets

374 The oldest joints, J1/J1*, found in the SW and NE of Bench IV (Fig. 13), fan out from a number of discrete
375 points on the faults and are continuous and longer than the outcrop dimensions (Figs. 3, 5, 9). In the domains
376 between the joint fans in Area E, there are areas completely devoid of J1* joints (Fig. 5). The local absence of
377 J1/ J1* joints could be due to lateral changes in the stress field or in lithology, but this cannot be resolved
378 without sampling and focussed local studies. In Area W, J1 joints show a small angle to J2 joints. Towards the
379 east, J1 gradually changes in orientation until it is indistinguishable from J2. In our interpretation J2 joints
380 formed late during the J1 phase, when the local minimum stress in the west of the bench rotated slightly
381 anticlockwise. Although J2 joints are only known from the western part of Area W, they may be distributed
382 throughout Bench IV as a later set of J1 joints, which can only be recognised where they make an angle with
383 older J1 joints. This problem is not inherent to joints; similar problems could be envisaged for the interference of
384 different sets of folds and foliations in other areas. J1 and J2 are quite similar and, thus, might be grouped in a
385 single generation, with single joints that have developed successively, but during the same event/stress field
386 orientation. Joints of sets J3 to J5 show a further gradual anticlockwise rotation after J1-J2 from NW-SE to NE-
387 SW and show an expansion of the area in which they develop to reach a maximum during J4 (Fig. 13). Despite
388 the fact that J3 and J4/J4* joints partly develop into pristine areas where now older joints were present, they are
389 of limited length (Fig. 8). J3 and J4/J4* joints are of similar length in areas with older J1 and J2 joints, and in
390 pristine areas, implying that the shorter length of the younger joints is not due to impingement on older
391 structures, but defined by other factors. J5/J5* joints, however, are significantly longer again than J3 and J4/J4*,
392 and crosscut earlier sets (Figs. 3, 8, 9). They occur in selected areas of the bench only (Fig. 13). J5* has a
393 fanning distribution similar but less extreme than J1/J1* joints (Fig. 9)

394 Sets J6/J6* and J7 have a significantly different orientation from preceding set J5 (Figs. 3, 8, 9) and occur in two
395 limited areas. Possibly, conditions for joint generation were similar in part of the outcrop during propagation of
396 J6-J7 in terms of the local lithology and layer thickness of Bench IV. Clearly, the break between sets J1-J5 and
397 J6-J7 is significant.

398 Joint spacing results show considerable variation in distribution, even within a certain set along different
399 scanlines, or even variations in frequency along a single scanline (Figs. 7, 8). Despite this variation, spacing is
400 relatively small for J2, J3, J6 and J7 joints, and larger for J1/J1*, J4/J4* and J5/J5*. There is no clear relation
401 between joint length and spacing (Fig. 8)

402 *4.5 X-intersections*

403 Most joint sets in this study can be classified as joint age sets or generations because of systematic abutment of
404 younger joints of similar orientation and length-spacing characteristics on older sets. Abutment is characterised
405 by a T-junction, where the younger joint does not cross over an older one, while in other cases the younger joint
406 changes direction close to the older joint, to impinge at higher angle than the far-field orientation (Figs. 4, 10).
407 Abutment is common when older joints are not sealed. Bench IV, however, shows many examples of
408 intersections where joints cross in so called X-intersections (Figs. 4, 10). X-intersections provide no information
409 on age relations, but are interesting, since they provide constraints on stress conditions during joint interaction
410 and on the nature of joint sealing (Renshaw and Pollard, 1995). In our dataset, X-intersections between joints
411 can occur at a very small angle, down to 5° (Fig. 10d). In Bench IV, X-intersections are especially common for
412 the older sets of joints, and one joint can commonly cross several older joints of even multiple sets before finally
413 abutting on a joint of an older set. The presence of such low angle X-intersections is intriguing, because if joints
414 are unsealed fractures, even with very high anisotropy of the horizontal stress, crosscutting is not possible at
415 such a low angle (Renshaw and Pollard, 1995): instead, the younger joints would abut on the older one without
416 crossing over into the adjacent block. However, joints can cross older joints if sealing of the older joint partly
417 restores the shear strength (Virgo et al., 2013, 2014, 2016; Laubach et al., 2019). If joints are completely
418 invisible to the stress field because they are sealed with vein material of exactly the same strength and elastic
419 modulus, joints can cross without any deflection. However, if mineralisation of joints is partial or if sectors of
420 joints are immobilised by jogs, so that these parts remain open and fluid filled, joints may cross older ones with
421 small deflections. In Bench IV of Lilstock, no macroscopic deflection is visible for most X-intersections, and we
422 propose that the older joints were at least partially sealed before the younger set crossed these. For most age sets,
423 joints cross several older joints before impinging on one of the same sets they crossed. This implies that joints
424 can propagate through partially sealed joints until they hit an unsealed section. The percentage of sealing in older
425 joints can therefore be expected to influence joint length of younger sets. Nevertheless, we saw no difference in
426 the length distribution of joints sets J3 and J4 between those propagating through previously jointed and
427 unjointed terrain (Figs. 3, 4c,d, 9). Their characteristic length may be explained by the nature of the stress-field
428 in Bench IV and the adjacent claystone layers, which must have been different from that during formation of the
429 long, early joints J1/J1* and J2. The excessive length of J5 joints compared to J4 and J3 can be partly due to the
430 fact that these joints form in domains where only short J4 joints formed previously, with locally relatively wide
431 spacing (Figs. 3, 13). All older joints, however, refractured before the formation of J8 and J8* joints, which
432 always abut on the older joints. An important conclusion from our observations is that, apart from J8-J8*, no set
433 of older joints will exclusively block propagation of a younger set; apparently, (partial) sealing of joints is
434 common in the subsurface. Microscopic investigation of un-weathered joints in the area could theoretically
435 provide information on sealing in future studies.

436 *4.6 Polyphase joints – reactivation: problems with abutment relations*

437 Our observations on abutment relations confirm earlier observations in other areas, that joints belonging to one
438 set may have formed in several time steps, and that some continuous joints are polyphase in nature (Pollard and
439 Aydin 1988; Alzayer et al., 2015). An example is seen in J4* and J6* joints, which impinge on each other while
440 the joint sets are clearly separated by J5* joints (Figs. 4e; 10a,b). Probably, some J4* joints were reactivated and
441 restarted growing with a new segments in the same orientation, to impinge on older parts of newly formed J6*
442 joints. This is a case where joints do not change orientation between active stages. Another observation showed
443 two J1 joints that apparently stopped growing, and were reactivated when J2 joints formed, with the new
444 segment following the direction of the second set with a sharp kink (Fig. 4b). The result is a rhomb-shaped form
445 defined by two sets of parallel J1 and J2 joints, mutually abutting. Polyphase joints can therefore be of two
446 types: those that continue growing in the same direction, since the stress field is similarly oriented, and those that
447 nucleate on the tip of older joints and propagate in a new direction. Such nucleation occurs in Bench IV up to an
448 angle of at least 17° (Fig. 4b). At larger angles the new, and in some cases, the old segments can open and form a
449 transition to pennant veins (Coelho et al., 2006) and wing cracks (Conçalves and Einstein, 2013; Kolari, 2017).
450 Finally, joints can nucleate in several directions at the same time. The youngest generation of veins (Fig. 10c)
451 shows an example where the recursive abutting of joints creates an “Escherian paradox” (Penrose and Penrose,
452 1958) where age relationships based on abutment criteria fails. We interpret this to indicate that the four joints
453 nucleated simultaneously and grew until abutting in the recursive set during uplift. This type of behaviour was
454 not observed for older joint sets.

455 *4.7 Joint length and age*

456 Because of the size of our study area, we were able to show that exceedingly long joints, up to 55 m in length,
457 exist as the oldest sets in the outcrop area, while J5 joints reach 40 m in length (Fig. 6). This is problematic for
458 other studies that use small outcrops or even drillcores for assessment of fracture networks. Fracture length is an
459 important parameter in fluid flow, especially in non-interconnected systems (Long and Witherspoon, 1985),
460 and the presence of such joints in the subsurface should be considered: the fact that the longest joints in Lilstock
461 are the oldest set, abutted by several later generations, implies that they are not an artefact of near surface
462 processes: they formed at the onset of joint formation in the rock volume under investigation, and are an integer
463 part of the original fracture content of the rock. Longer joints have also been observed by Laubach et al., (2016)
464 and surface mapping as advocated in this paper could be the only way to assess the importance of long fractures,
465 and to find criteria to recognise them in cross-section in the subsurface.

466 *4.8. Joint curvature*

467 J1/J1* and J5 joints form fans focussing on a fault on the southern side of the exposed part of Bench IV (Figs. 3,
468 5, 9). Rawnsley et al. (1998), has shown that the fans of J1* joints converge on asperities on faults. Some of the
469 long J1* joints are strongly curved. Short J1* joints are less sinuous than the longer ones, which might be due to
470 mechanical effects, e.g., segmental growth of longer fractures causing a higher curvature, or the tendency to fan
471 out and curve more within a larger distance from the source (in this case the proximate fault) that causes the

472 local stress field leading to the fracturing. The same may apply to J5* joints, which tend to be straighter and
473 shorter than J1* joints.

474 *4.9. The recognition of joint generations versus sets*

475 Although we were able to recognise eight sets of joints, it is unclear if these can be grouped into generations or
476 deformation phases in the classical sense. Joint generations J1-J5 show a gradual clockwise change in orientation
477 from NW to NE trending (Fig. 8). On the other hand, J1 and J5 joints show curvature and fanning geometries,
478 while the other joint sets J2-J3 and J4 are straight (Figs. 3, 9). Joints sets J6 and J7 only occur locally and are of
479 very different orientation as the older ones and may form a separate generation (Figs. 5, 13). J5 joints may form
480 the transition between these two main groups. J8, finally, is definitely quite different from the other joints, and
481 form a separate generation. The joint sets could therefore be grouped into three main age groups, J1-J5; J6-J7;
482 and J8. Although joints can be relatively dated in one location, it is uncertain how diachronous they are, even
483 within the platform of layer IV. In this discussion, we have shown that mapping of small outcrops, or worse, drill
484 cores, may provide insufficient information to correctly assess the fracture network present in any area, and may
485 tend to oversimplify the interpreted fracture history.

486 **5. Conclusions**

- 487 1) Using our method of UAV-based photography and image processing, it is possible to obtain sufficient
488 resolution to characterise the full fracture content of large outcrops, such as the Lilstock benches.
- 489 2) The Lilstock outcrop in the Bristol Channel shows evidence for eight sets of joints, up to six in each
490 location on a 25 m² scale. These sets are distinguished by a fixed set of criteria, set up for this study but
491 generally applicable.
- 492 3) Different stratigraphic layers have different sets of joints. Most layers have 2-3 and only one layer (IV),
493 with maximum thickness, has 8 sets and at least four generations over most of the area
- 494 4) It is impossible to recognise the full array of joint sets in small outcrops (25 m² or smaller) in the
495 Lilstock Bench IV: six sets is the maximum in any such domains. This places significant restrictions on
496 the use of small outcrops or, worse, drill cores for the reconstruction of fracture networks.
- 497 5) Joint sets cannot be recognized exclusively by their orientation and cannot always be distinguished if
498 they fan into parallelism.
- 499 6) Most of the joint sets mapped probably formed in the subsurface, not during final uplift and exposure at
500 the surface.
- 501 7) Crosscutting of one set of joints by the next mostly occurs in older joint sets. The youngest set does not
502 commonly cross older joints, probably because these older joints are opening with uplift. The youngest
503 set of joints (J8 and J8*) has only T-junctions
- 504 8) Joints of one set can terminate on older joints or cross them, creating X- or T-junctions
- 505 9) Joints can cross other joints at very small angles, down to 5°, without deflection. This is interpreted to
506 mean that such older joints were mechanically inactive, and invisible in the stress field
- 507 10) Joints can be polyphase, with segments that belong to different age generations

508 **Acknowledgements**

509 Funding: JLU and MP thank the German Science Foundation DFG for funding this project (grants UR 64/17-1).

510 **References**

- 511 ALZAYER, Y., EICHHUBL, P. and LAUBACH, S.E. 2015. Non-linear growth kinematics of opening-mode
512 fractures. *Journal of Structural Geology*, 74, 31-44.
- 513 BELAYNEH, M. 2003. Analysis of natural fracture networks in massive and well-bedded carbonates and the
514 impact of these networks on fluid flow in dual porosity modelling. Thesis, Imperial College London
515 (University of London).
- 516 BELAYNEH, M. 2004. Palaeostress orientation inferred from surface morphology of joints on the southern
517 margin of the Bristol Channel Basin, UK. Geological Society, London, Special Publications, 231, 243-
518 255.
- 519 BELAYNEH, M. and COSGROVE, J.W. 2004. Fracture-pattern variations around a major fold and their
520 implications regarding fracture prediction using limited data: an example from the Bristol Channel Basin.
521 Geological Society, London, Special Publications, 231, 89-102.
- 522 BELAYNEH, M., GEIGER, S. and MATTHÄI, S.K. 2006. Numerical simulation of water injection into layered
523 fractured carbonate reservoir analogs. *AAPG Bulletin*, 90, 1473-1493.
- 524 BERKOWITZ, B. 2002. Characterizing flow and transport in fractured geological media: A review. *Advances in*
525 *Water Resources*, 25, 861-884.
- 526 BONNET, E., BOUR, O., ODLING, N.E., DAVY, P., MAIN, I., COWIE, P. and BERKOWITZ, B. 2001.
527 Scaling of fracture systems in geological media. *Reviews of Geophysics*, 39, 347-383.
- 528 BOURNE, S. J. and WILLEMSE, E. J. M. 2001. Elastic stress control on the pattern of tensile fracturing around
529 a small fault network at Nash Point, UK. *Journal of Structural Geology* 23, 1753-1770
- 530 BROOKS, M., TRAYNER, P.M. and TRIMBLE, T.J. 1988. Mesozoic reactivation of Variscan thrusting in the
531 Bristol Channel area, UK. *Journal of the Geological Society*, 145, 439-444.
- 532 BOURNE, S.J. 2003. Contrast of elastic properties between rock layers as a mechanism for the initiation and
533 orientation of tensile failure under uniform remote compression. *Journal of Geophysical Research: Solid*
534 *Earth*, 108, p. 2395
- 535 CAPUTO, R. and HANCOCK, P.L. 1999. Crack-jump mechanism and its implications for stress cyclicity
536 during extension fracturing. *Journal of Geodynamics*, 27, 45-60.
- 537 CHADWICK, R.A. 1993. Aspects of basin inversion in southern Britain. *Journal of the Geological Society*,
538 London, 150, 311-322.
- 539 COELHO, S., PASSCHIER, C., MARQUES, F. 2006. Riedel-shear control on the development of pennant
540 veins: Field example and analogue modelling. *Journal of Structural Geology*, 28, 1658-1669.
- 541 CONÇALVES DA SILVA, B. and EINSTEIN, H. H. 2013. Modeling of crack initiation, propagation and
542 coalescence in rocks. *International Journal of Fracture* 257563978. DOI 10.1007/s10704-013-9866-8

543 COSGROVE, J.W. 2001. Hydraulic fracturing during the formation and deformation of a basin: a factor in the
544 dewatering of low-permeability sediments. *AAPG Bulletin*, 85, 737-748.

545 DART, C.J., MCCLAY, K. and HOLLINGS, P.N. 1995. 3D analysis of inverted extensional fault systems,
546 southern Bristol Channel basin. *In: Buchanan J.G. and Buchanan P.G. Basin Inversion*, (ed.), Geological
547 Society Special, 88, 393-413.

548 DAVISON, I. 1995. Fault slip evolution determined from crack-seal veins in pull-aparts and their implications
549 for general slip models. *Journal of Structural Geology*, 17, 1025-1034.

550 De DREUZY, J.-R., MÉHEUST, Y. and PICHOT, G. 2012. Influence of fracture scale heterogeneity on the flow
551 properties of three-dimensional discrete fracture networks (DFN). *Journal of Geophysical Research: Solid*
552 *Earth*, 117, B11207

553 DERSHOWITZ, W.S. and HERDA, H.H. 1992. Interpretation of fracture spacing and intensity. *In: The 33th*
554 *U.S. Symposium on Rock Mechanics (USRMS)*, p. 10, Santa Fe, New Mexico.

555 DYER, R. 1998. Using joint interactions to estimate paleostress ratios. *Journal of Structural Geology*, 10, 685–
556 699.

557 ENGELDER, T. and PEACOCK, D.C.P 2001. Joint development normal to regional compression during
558 flexural-flow folding: the Lilstock buttress anticline, Somerset, England. *Journal of Structural Geology*,
559 23, 259-277.

560 FOSSEN, H. 2016. *Structural Geology*. Cambridge University Press, 510pp.

561 GILLESPIE, P., MONSEN, E., MAERTEN, L., HUNT, D., THURMOND, J. and TUCK, D. 2011. Fractures in
562 carbonates: from digital outcrops to mechanical models. *Society for Sedimentary Geology*, 10, 137-147.

563 GLEN, R.A., HANCOCK, P.L. and WHITTAKER, A. 2005. Basin inversion by distributed deformation: the
564 southern margin of the Bristol Channel Basin, England. *Journal of Structural Geology*, 27, 2113-2134.

565 KELLY, R.G., SANDERSON, D.J. and PEACOCK, D.C.P. 1998. Linkage and evolution of conjugate strike-slip
566 fault zones in limestones of Somerset and Northumbria. *Journal of Structural Geology*, 20, 1447-1493.

567 KELLY, P.G., PEACOCK, D.C.P, SANDERSON, D.J. and MCGURK, A.C. 1999. Selective reverse-
568 reactivation of normal faults, deformation around reverse-reactivated faults in the Mesozoic of the
569 Somerset coast. *Journal of Structural Geology*, 21, 493-509.

570 KOLARI, K. 2017. A complete three-dimensional continuum model of wing-crack growth in granular brittle
571 solids. *International Journal of Solids and Structures* 115-116, 27-42.

572 LAUBACH, S.E., FALL, A., COPLEY, L.K., MARRETT, R. and WILKINS, S.K. 2016. Fracture porosity
573 creation and persistence in a basement-involved Laramide fold, Upper Cretaceous Frontier Formation,
574 Green River Basin, USA. *Geological Magazine*, 153, 887-910.

575 LAUBACH, S.E., LANDER, R.H., CRISCENTI, L.J. ANOVITZ, L.M., URAI, J.L., POLLYEA, R.M.,
576 HOOKER, J.N., NARR, W. EVANS, M.A., KERISIT, S.N., OLSON, J.E., DEWERS, T., FISHER, D.,
577 BODNAR, R., EVANS, B., DOVE, P., BONNELL, L.M., MARDER, M.P. and PYRAK-NOLTE, L.
578 2019. The Role of Chemistry in Fracture Pattern Development and Opportunities to Advance
579 Interpretations of Geological Materials. *Reviews of Geophysics*, 57, 1065-1111.

580 LONG, J.C.S. and WITHERSPOON, P.A. 1985. The relationship of the degree of interconnection to
581 permeability in fracture networks. *Journal of Geophysical Research: Solid Earth*, 90, 3087-3098.

582 LOOSVELD, R.J.H. and FRANSEN, R.C.M.W. 1992. Extensional vs. shear fractures: implications for
583 reservoir characterisation. *Society of Petroleum Engineers, SPE 25017*, 23-30. Nemčok and Gayer 1996

584 LORENZ, J. C., STERLING, J. L., SCHECHTER, D. S., WHIGHAM, C. L., and JENSEN, J. L. (2002).
585 Natural fractures in the Spraberry Formation, Midland basin, Texas: The effects of mechanical
586 stratigraphy on fracture variability and reservoir behavior. *AAPG Bulletin*, 86(3), 505-524.

587 MAERTEN, L, MAERTEN, F, LEJRI, M. 2018. Along fault friction and fluid pressure effects on the spatial
588 distribution of fault-related fractures *Journal of Structural Geology*, 108, 198-212.

589 MANDL, G. 2005. *Rock joints: their mechanical genesis*. Springer-Verlag, 221pp.

590 MENEGONI, N., MEISINA, C., PEROTTI, C. and CROZI, M. 2018. Analysis by UAV Digital
591 Photogrammetry of Folds and Related Fractures in the Monte Antola Flysch Formation (Ponte
592 Organasco, Italy). *Geosciences*, 8, 299.

593 NEMČOK, M., GAYER, R. and MILIORIZOS, M. 1995. Structural analysis of the inverted Bristol Channel
594 Basin: implications for the geometry and timing of fracture porosity. *In: Buchanan, J.G. and Buchanan,*
595 *P.G., (ed.), Basin Inversion*. Geological Society, London, Special Publications, 88, 355-392.

596 NEMČOK, M. and GAYER, R. 1996. Modelling palaeostress magnitude and age in extensional basins: a case
597 study from the Mesozoic Bristol Channel Basin, U.K. *Journal of Structural Geology*, 18, 1301-1314.

598 NYBERG, B., NIXON, C. W. and SANDERSON, D. J. 2018. NetworkGT: A GIS tool for geometric and
599 topological analysis of two-dimensional fracture networks. *Geosphere*, 14(4), 1618–1634

600 OLSON, J.E., LAUBACH, S.E. and LANDER, R.H. 2009. Natural fracture characterization in tight gas
601 sandstones: Integrating mechanics and diagenesis. *AAPG Bulletin*, 93, 1535–1549.

602 PEACOCK, D.C.P. and SANDERSON, D.J. 1991. Displacements, segment linkage and relay ramps in normal
603 fault zones. *Journal of Structural Geology*, 13, 721-733.

604 PEACOCK, D.C.P. and SANDERSON, D.J. 1994. Geometry and development of relay ramps in normal fault
605 systems. *AAPG Bulletin*, 78, 147-165.

606 PEACOCK, D.C.P. and SANDERSON, D.J. 1995. Strike-slip relay ramps. *Journal of Structural Geology*, 17,
607 1351-1360.

608 PEACOCK, D.C.P. 2001. The temporal relationship between joints and faults. *Journal of Structural Geology*,
609 23, 329-341.

610 PEACOCK, D.C.P. 2004. Differences between veins and joints using the example of the Jurassic limestones of
611 Somerset. *In: Cosgrove J.W. and Engelder T. The Initiation, Propagation, and Arrest of Joints and Other*
612 *Fractures*, (ed.), Geological Society, London, Special Publications, 231, 209-221.

613 PEACOCK, D.C.P., SANDERSON, D.J. and ROTEVATN, A. 2018. Relationships between fractures. *Journal*
614 *of Structural Geology*, 106, 41–53.

615 PENROSE, L. S. and PENROSE, R. 1958. Impossible objects: a special type of visual illusion. *British Journal*
616 *of Psychology*, 49, 31-33.

617 POLLARD, D.D and AYDIN, A. 1988. Progress in understanding jointing over the past century. *GSA Bulletin*
618 100, 1181–1204.

619 POLLYEA, R.M. and FAIRLEY, J.P. 2011. Estimating surface roughness of terrestrial laser scan data using
620 orthogonal distance regression. *Geology*, 39, 623–626.

621 PRICE, N.J. and COSGROVE, J.W. 1990. *Analysis of Geological Structures*. Cambridge University Press,
622 502pp.

623 PYRAK-NOLTE, L.J. and DePAOLO, D.J. 2015. Controlling Subsurface Fractures and Fluid Flow: A Basic
624 Research Agenda. United States. <https://doi.org/10.2172/1283189>

625 RAWNSLEY, K.D., PEACOCK, D.C.P., RIVES, T. and PETIT, J.-P. 1998. Joints in the Mesozoic sediments
626 around the Bristol Channel Basin. *Journal of Structural Geology*, 20, 1641-1661.

627 RENSHAW, C.E. and POLLARD, D.D. 1995. An experimentally verified criterion for propagation across
628 unbounded frictional interfaces in brittle, linear elastic materials. *International Journal of Rock*
629 *Mechanics and Mining Sciences and Geomechanics Abstracts*, 32, 237-249.

630 TSANG, C.-F. and NERETNIEKS, I. 1998. Flow channeling in heterogeneous fractured rocks. *Reviews of*
631 *Geophysics*, 36, 275-298.

632 TWISS, R.J. and MOORES, E.M. 1992. *Structural geology*. Freeman, New York, 531pp.

633 VIRGO, S., ARNDT, M., SOBISCH, Z., URAI, J.L. 2013. Development of fault and vein networks in a
634 carbonate sequence near Hayl al-Shaz, Oman Mountains. *GeoArabia*, 18, 99-136.

635 VIRGO, S. ABE, S. and URAI, J.L. 2014. The evolution of crack seal vein and fracture networks in an evolving
636 stress field: Insights from Discrete Element Models of fracture sealing. *Journal of Geophysical Research:*
637 *Solid Earth*, 119, 8708-8727.

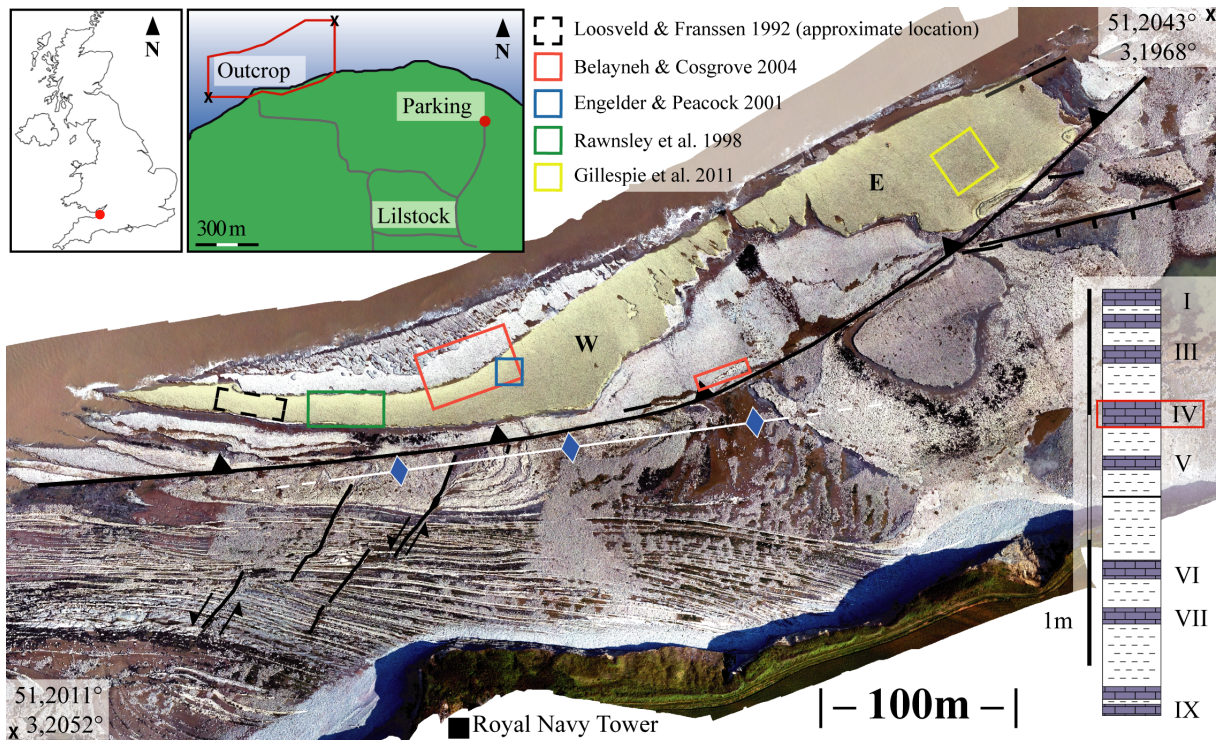
638 VIRGO, S. ABE, S. and URAI, J.L. 2016. The influence of loading conditions on fracture initiation,
639 propagation, and interaction in rocks with veins: Results from a comparative Discrete Element Method
640 study. *Journal of Geophysical Research: Solid Earth*, 121, 1730-1738.

641 WEISMÜLLER, C., PRABHAKARAN, R., PASSCHIER, M., URAI, J.L., BERTOTTI, G. and REICHERTER,
642 K. 2020a. Mapping the fracture network in the Lilstock pavement, Bristol Channel, UK: manual versus
643 automatic. *Solid Earth*, 11, 1773–1802, <https://doi.org/10.5194/se-11-1773-2020>.

644 WEISMÜLLER, C., PASSCHIER, M., URAI, J.L. and REICHERTER, K, 2020b: The fracture network in the
645 Lilstock pavement, Bristol Channel, UK: digital elevation models and orthorectified mosaics created
646 from unmanned aerial vehicle imagery, RWTH Aachen University Library, DOI: 10.18154/RWTH-2020-
647 06903

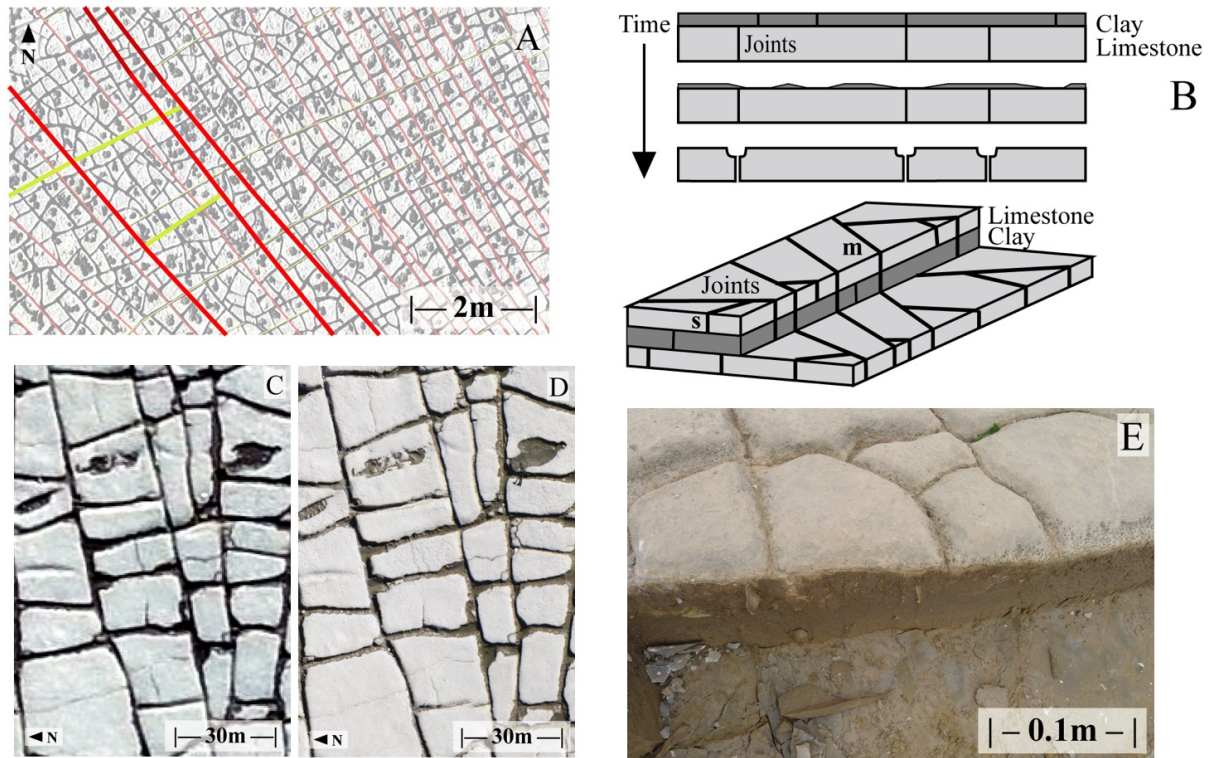
648 WILLEMSE, E.J.M. 1997. Segmented normal faults: Correspondence between three-dimensional mechanical
649 models and field data. *Journal of Geophysical Research: Solid Earth*, 102, 675-692.

650 WÜSTEFELD, P., De MEDEIROS, M., KOEHRER, B., SIBBING, D., KOBBELT, L. and HILGERS, C. 2018.
651 Evaluation of a workflow to derive terrestrial light detection and ranging fracture statistics of a tight gas
652 sandstone reservoir analog. *AAPG Bulletin*, 102, 2355–2387.



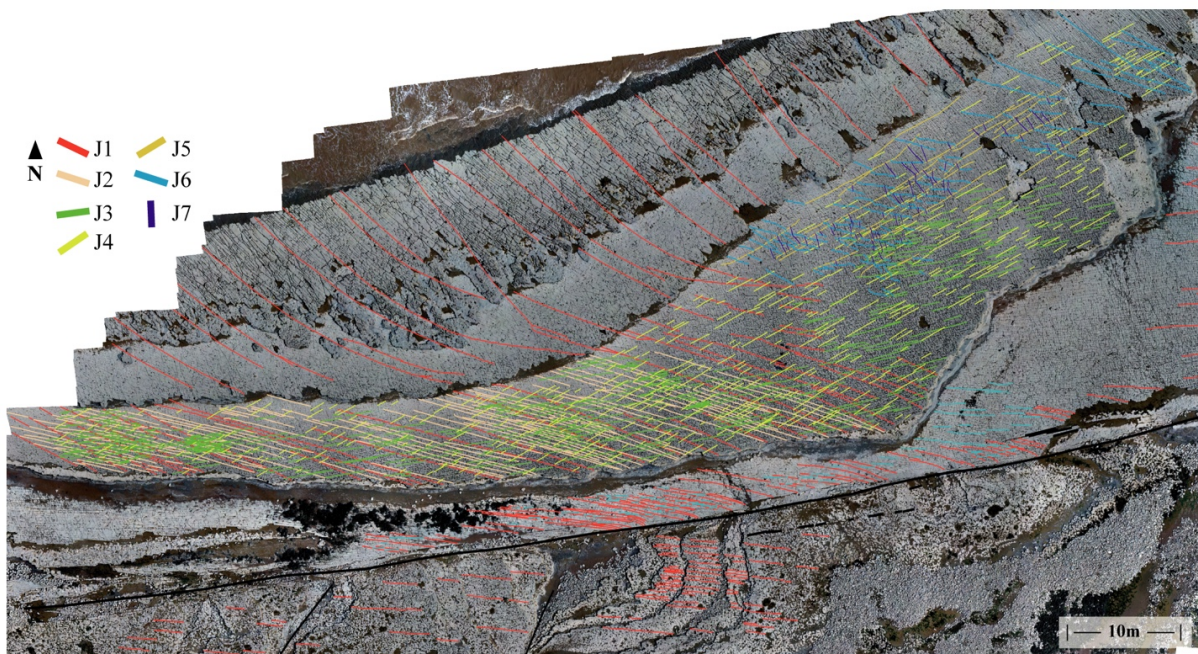
653

654 **Fig. 1.** Overview of the main part of the Lilstock Benches in a merged digital image, taken from 100m altitude.
 655 Bench IV, an outcropping part of layer IV is highlighted in yellow, the main faults in black, the anticline in
 656 white with blue arrows. W and E: Areas W and E of Bench IV. Locations of previous work on joints in the
 657 literature shown as coloured rectangles. Location of Lilstock in the UK and the outcrop at Lilstock Beach,
 658 outlined in red shown in insets at top left. Stratigraphic column of the clay and limestone benches shown at
 659 bottom right, highlighting layer IV.



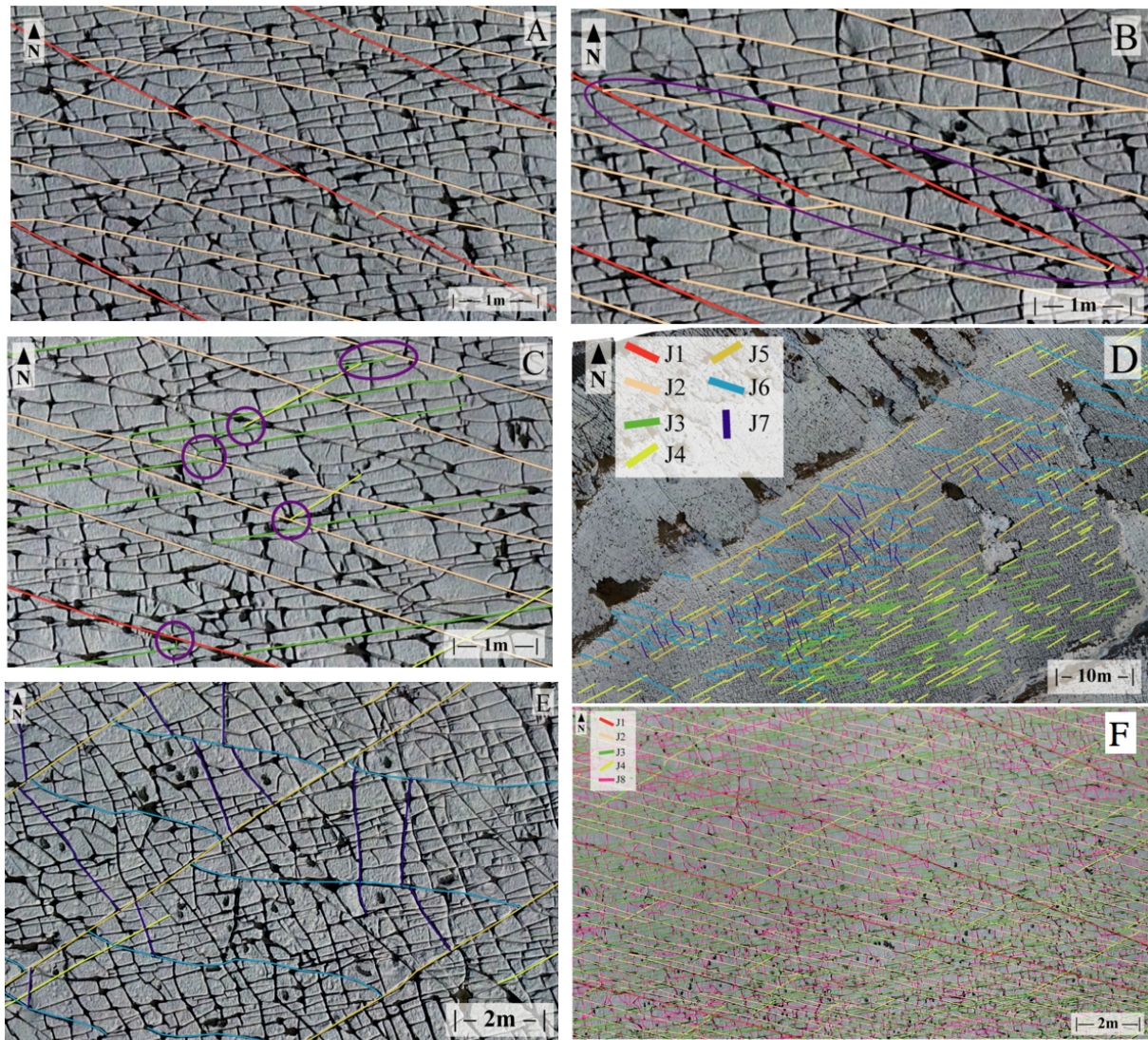
660

661 **Fig. 2.** (a) example of T- and X-junctions between J1* (red) and J4* (yellow) joints in Area E. (b) weathering
 662 process erodes joints to a “U” shape that makes them visible from a distance. Joint can be formed within only
 663 one layer (s) or can cross into multiple layers above and below (m). (c) resolution of 7.4mm pixel used for this
 664 study compared to (d) the resolution of field photography with 2.2mm pixel size. (e) field photo of typical
 665 eroded joints of Bench IV.



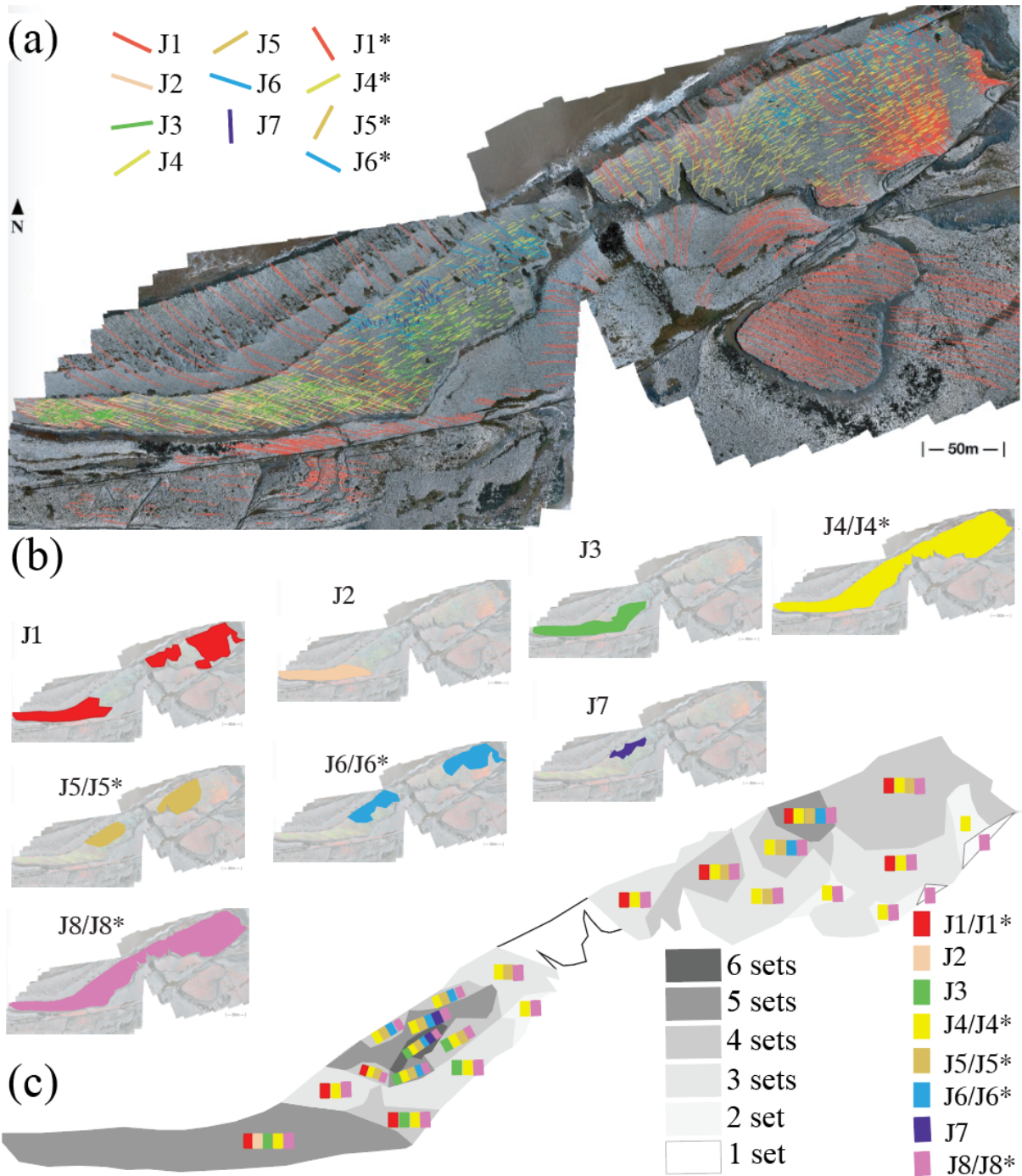
666

667 **Fig. 3.** Overview of Area W with all mapped sets marked in colour, except for the youngest, J8. Visible are J1
 668 and J2 approaching sub-parallelism in the centre of the layer and the local aspect of some sets.



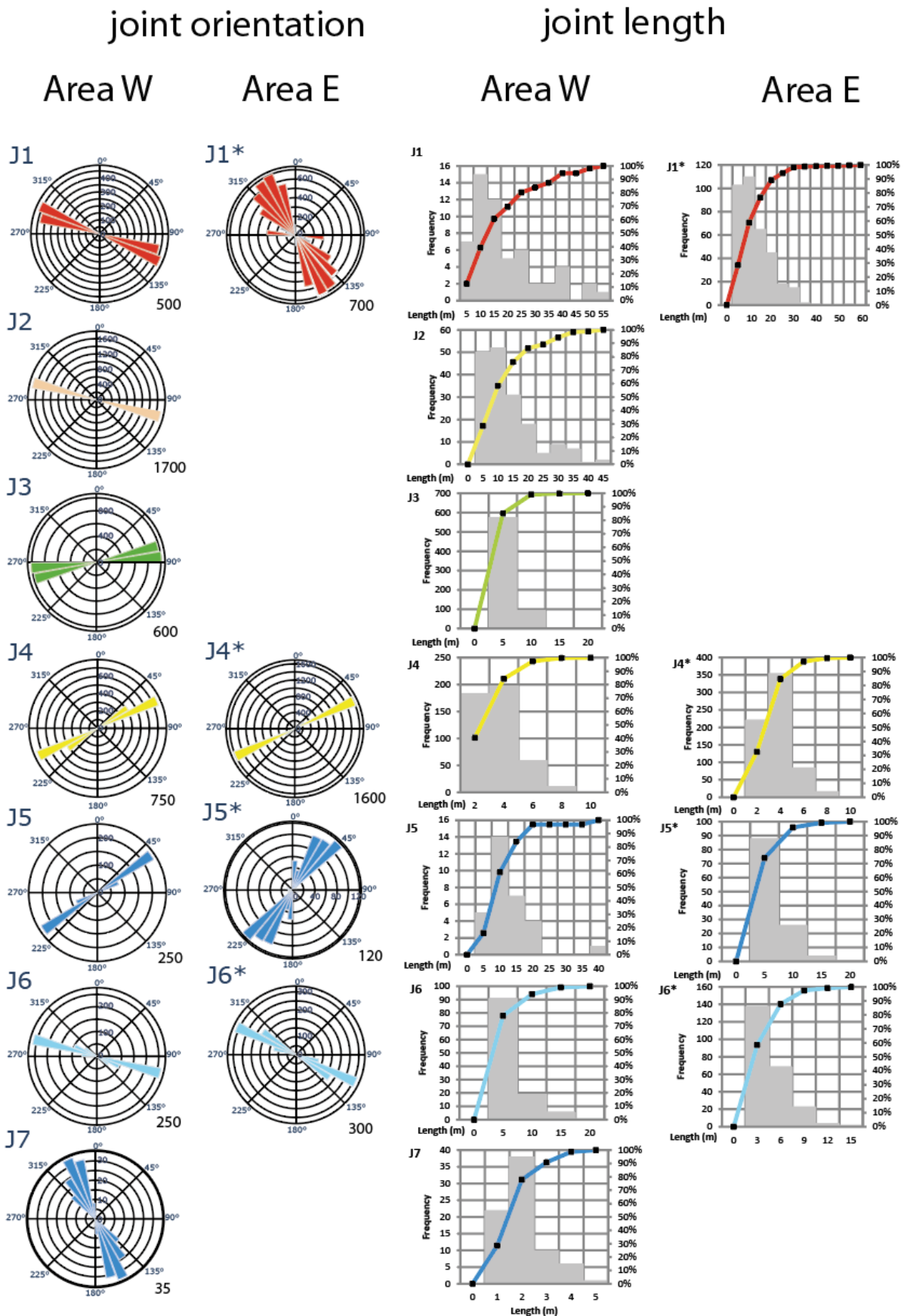
669

670 **Fig. 4.** Interaction of different sets of joints in Area W. Selected joints have been marked in colour for clarity. (a)
 671 J2 joints (beige) of Area W abut on J1 joints (red). J3 and J4 joints are visible but have not been colour-coded.
 672 (b) rhomb shaped form (marked by pink oval) defined by J1 and J2 joints, caused by mutual impingement,
 673 probably due to reactivation of J1 joints during formation of J2 joints. (c) abutment relations of sets J1 (red), J2
 674 (beige), J3 (green) and J4 (yellow) joints in Area W. Pink circles show abutment. (d) enlarged north-eastern part
 675 of Area W with locally occurring sets: J5, J6 and J7. The more widely distributed sets J3 and J4 are also present,
 676 while J1 and J2 are not developed in this location. (e) strongly curved J6 joints (light blue) impinging on J5
 677 (yellow). J7 joints dark blue. Curvature is such that it increases the impingement angle. (f) section of outcrop
 678 with all joints highlighted: J1-J4 and J8 (enlarged in Fig. S2).



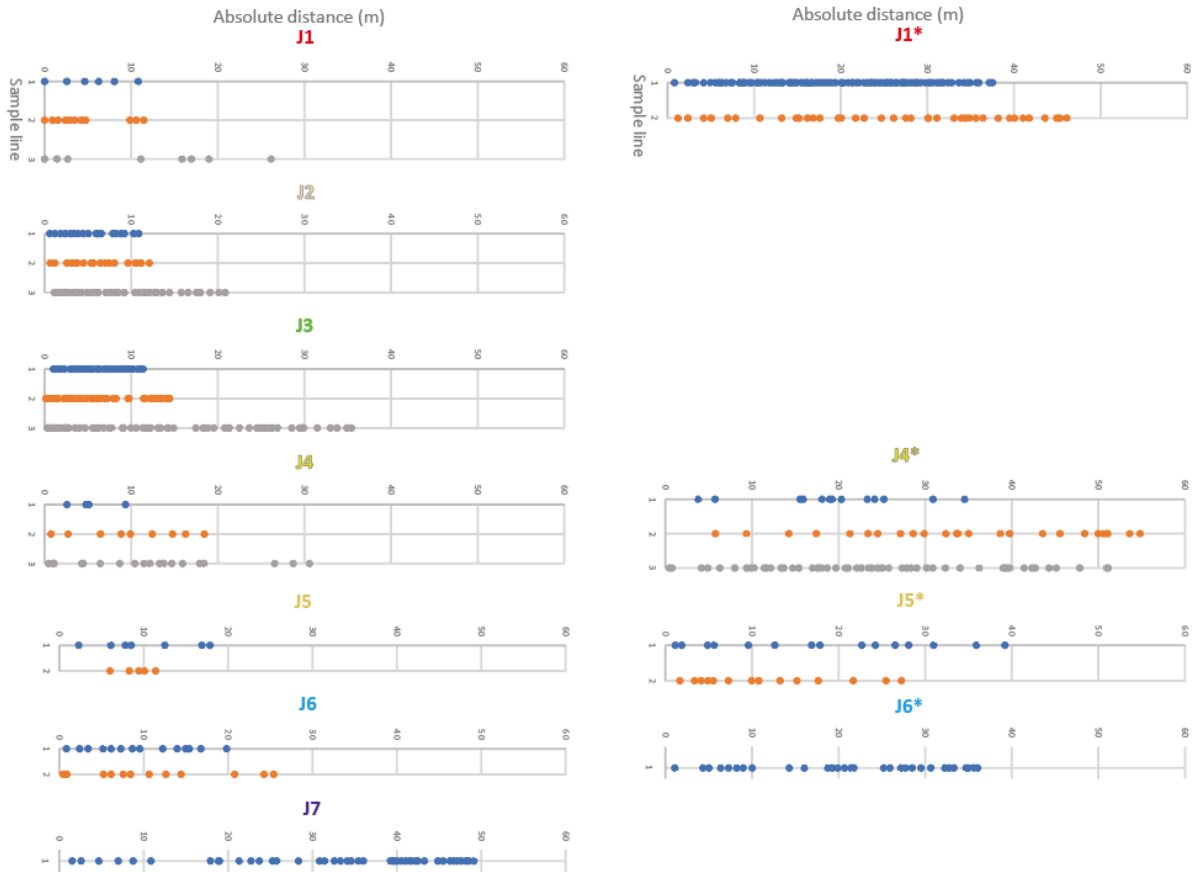
679

680 **Fig. 5.** Distribution of all joints over Bench IV. Joint set J8 not shown. (a) general distribution of joint sets.
 681 Enlargement with higher resolution in Supplementary Fig. S1. (b) spatial distribution of the individual sets. (c)
 682 approximate distribution of the number of sets present over bench IV. The maximum number of joints in any
 683 domain is six, including set J8. Coloured bars indicate the joint sets present in each domain.



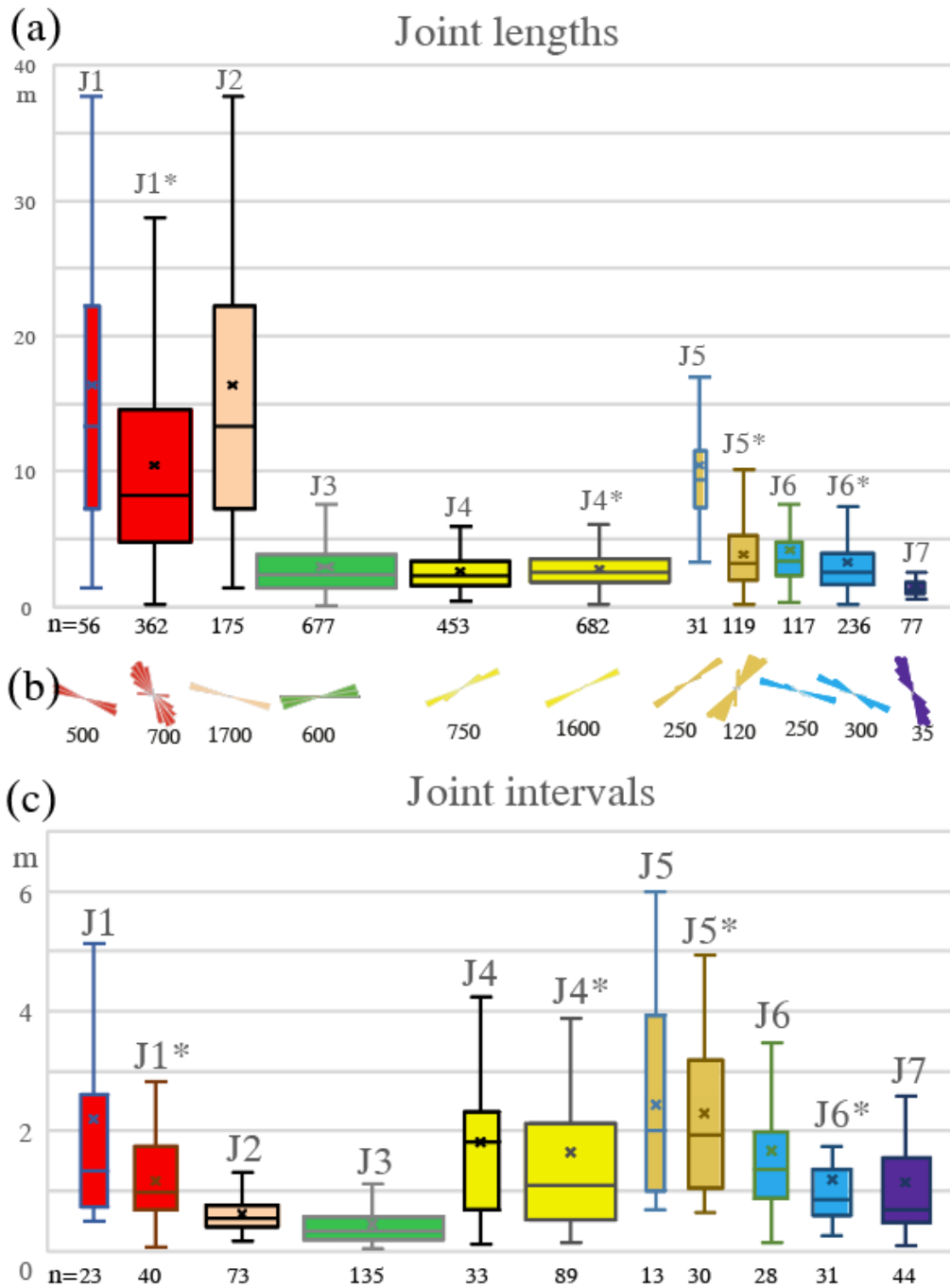
684
685
686

Fig. 6. Length-weighted rose diagrams with a bin size of 10° for Joint populations and histogram and cumulative length distribution of joints sorted by set. Data in Table 2



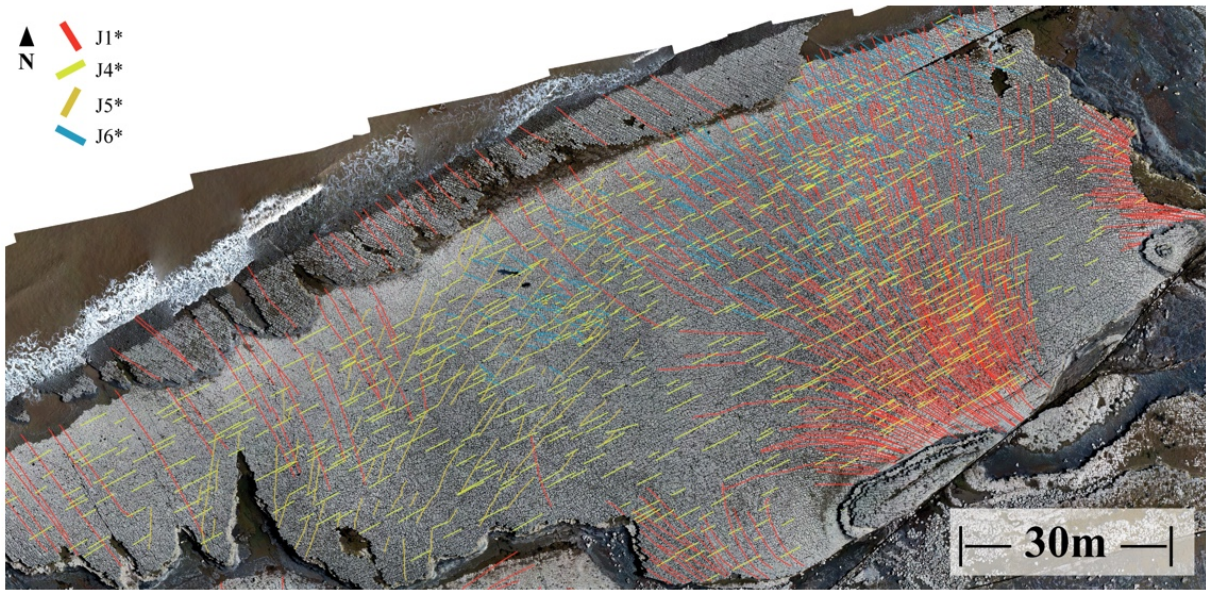
687

688 **Fig. 7.** Joint spacing along scanlines oriented 90° to the average strike of the respective joint set.



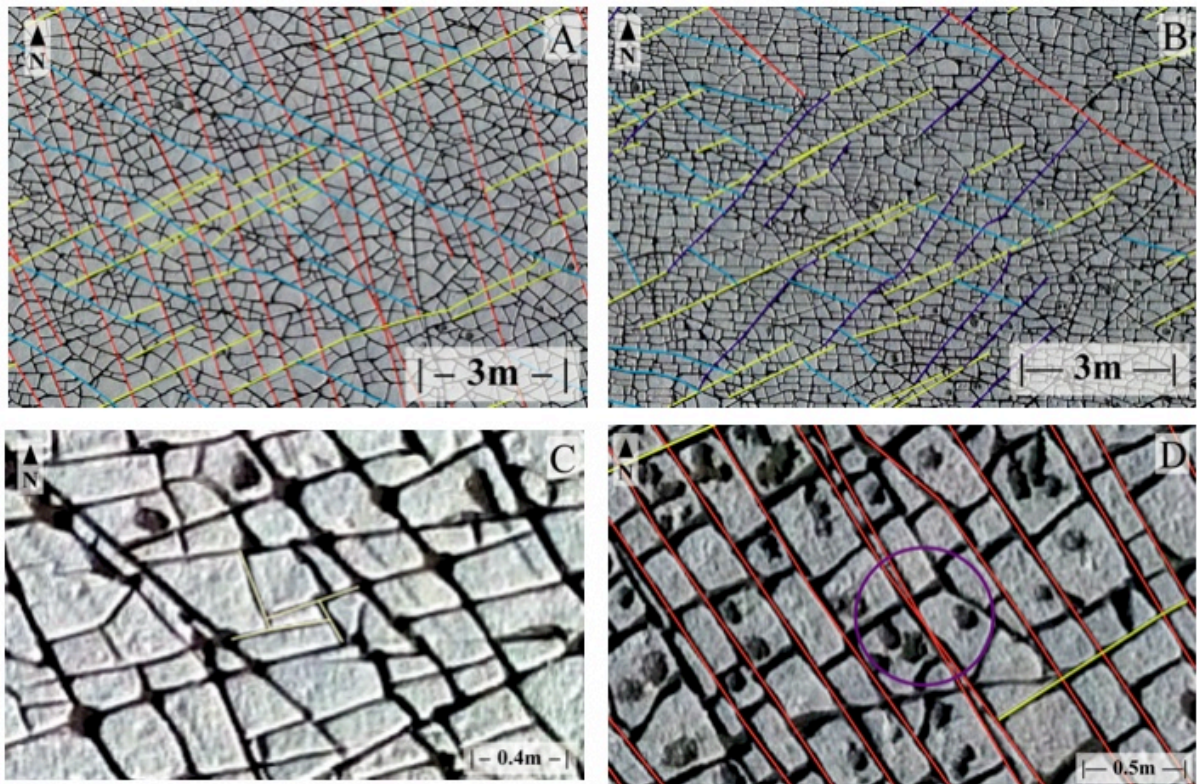
689

690 **Fig. 8.** (a) box and whisker plots of joint length for all joint sets, with outliers left out. (b) summarised
 691 orientation diagrams of the joint sets, based on Figure 6a, for comparison. (c) box and whisker plots of joint
 692 intervals measured along profiles as shown in Figure 7.



693

694 **Fig. 9.** Overview of Area E with all mapped joint sets except the youngest J8*. J5* and J6* occur mostly in
 695 separate locations with only a small area of overlap.



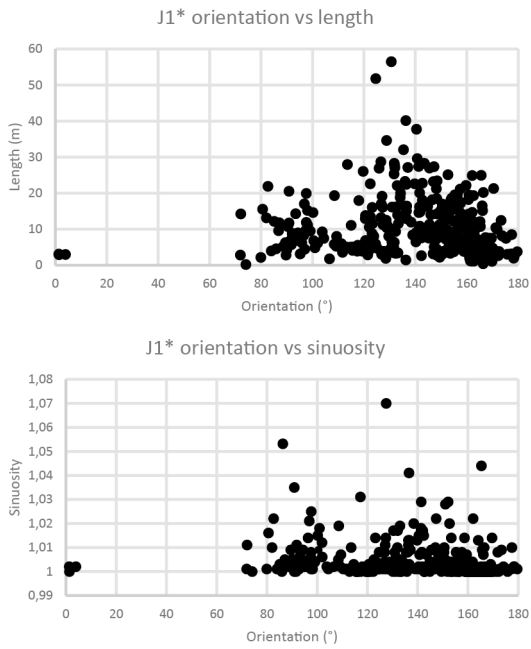
696

697 **Fig. 10.** Interaction of different sets of joints mostly from Area E. Selected joints have been marked in colour for
 698 clarity. (a) apparently conflicting abutting relations between J4* (yellow) and J6* (light blue). These sets are
 699 abutting each other with equal frequency. (b) J6* abutting J5*, which abuts to J4* resolving the age-relationship.
 700 (c) four J8 joints from Area A forming an Escherian paradox through T-intersections that contradict the simple
 701 analysis based on sequential joint growth. (d) the smallest angle of crossing joints could be observed between
 702 two J1* joints at 5° (marked by a circle).



703

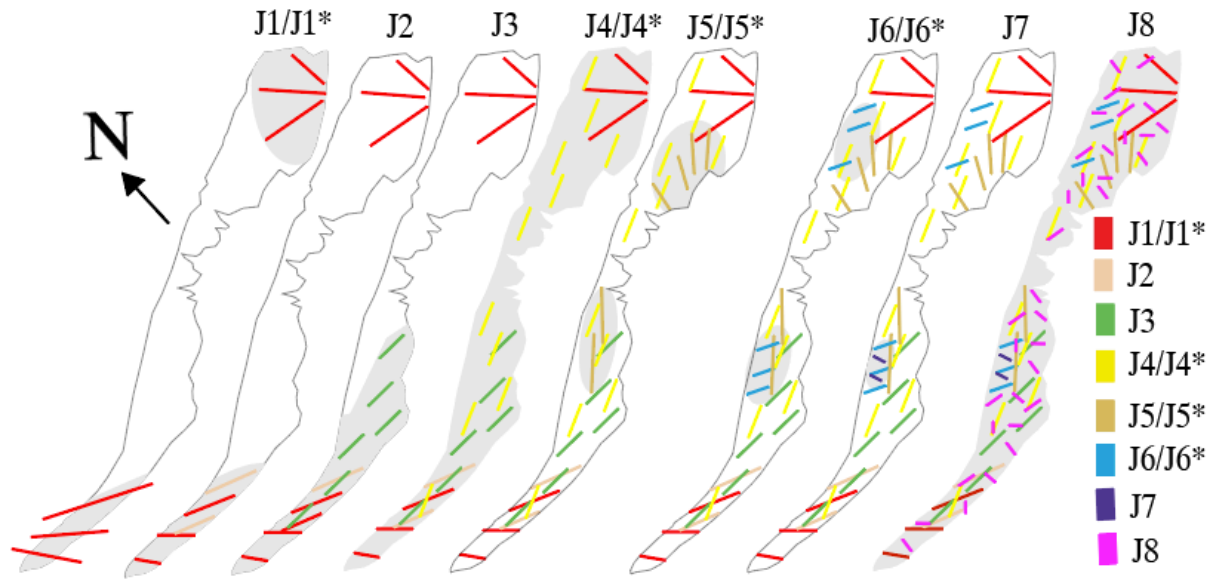
704 **Fig. 11.** Joint trace curvature map of J1* in Area E. Increasing curvature is indicated by increasingly dark red
 705 colour of joints



706

707 **Fig. 12.** Plots showing the relation of orientation and length as well as orientation and curvature for J1* joints.

708



709

710

Fig. 13. Development of the subsequent joint sets in Bench IV. Coloured bars schematically indicate the orientation and relative length of joint sets. Grey background indicates the area of active development of each set

East		West		Generations in literature			
Generation Strike Length [m]	Curvature Properties	Generation Strike Length [m]	Curvature Properties	B&C	E&P	L&F	Rea
J1 115-120° 30-50	straight	J1* 300-340° 10-30	fanning out connected to fault	J1 115- 120°	J2 115- 120°	1	3 125- 130°
J2 100-105° 6-10	straight, curve into T junction			J2 110- 115°	J4 95- 105°	2	4 100- 110°
J3 80° 6-15	straight, most common			J3 85- 95°	J6 75- 85°	3&4	
J4 60° 1-4	straight consistent	J4* 60-65° 1-6	straight consistent	J4 65- 70°		5	
J5 55-60° 10-20	lightly curved local presence	J5* 5-40° 2-5	straight				
J6 100-110° 4-8	strongly curved local presence	J6* 110-130° 1-3	slightly curved				
J7 340-10° 2-5	straight local presence			J6 335- 345°			
J8 variable <0.5	curvy irregular	J8* variable <0.5	straight				

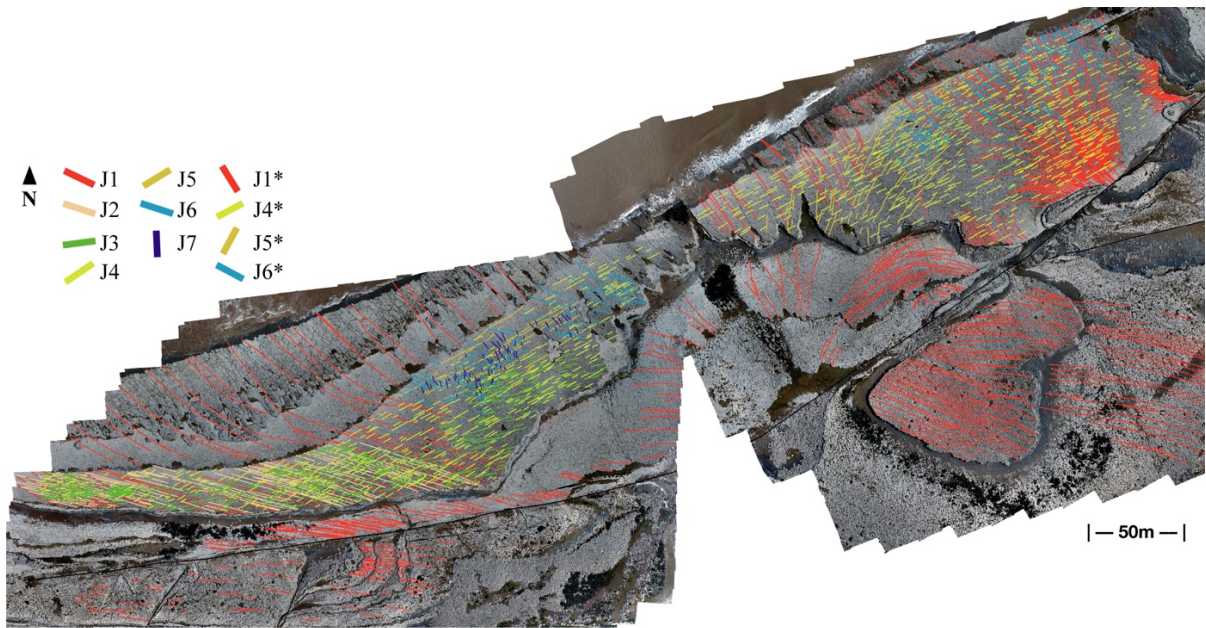
711

712 **Table 1.** Joint sets and their characteristics in Areas W and E, as well as the connections that can be observed
713 between sets in both areas. Included at the right side are joint sets described in other publications that can be
714 related to sets identified here. Non assignable sets are omitted, strike-values are given if provided in the
715 literature. B&C - Belayneh and Cosgrove (2004); E&P - Engelder and Peacock (2001); L&F - Loosveld and
716 Franssen (1992); Rea - Rawnsley et al., (1998).

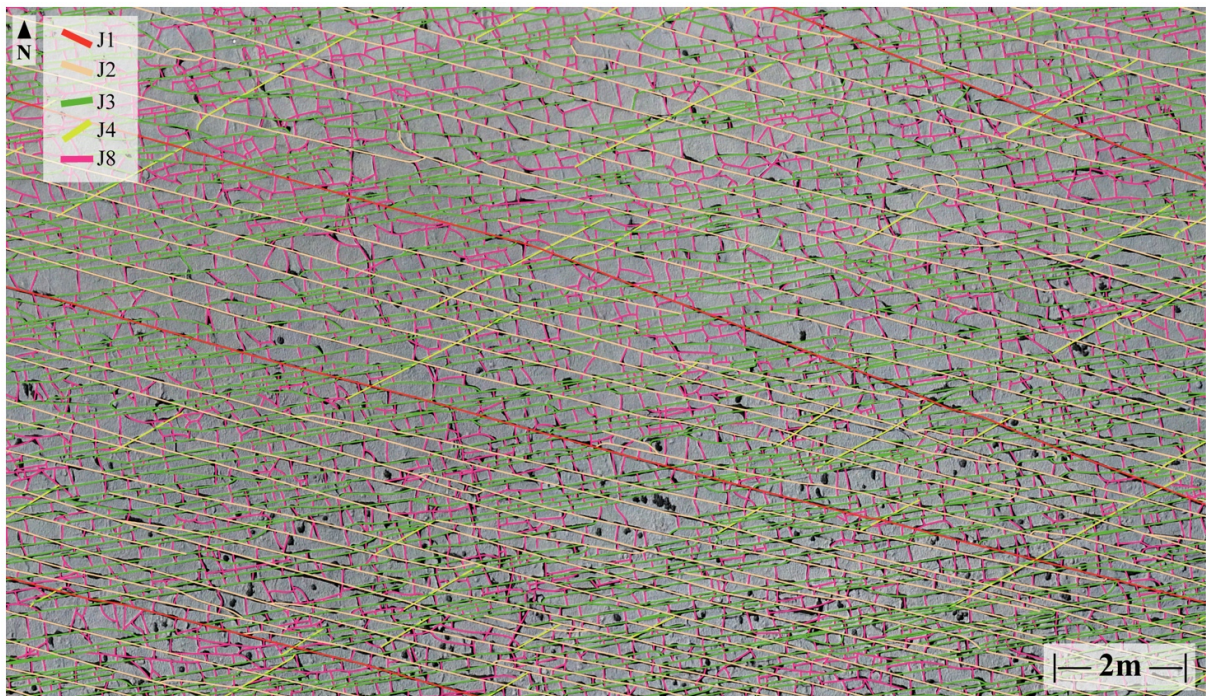
		Area W	J1	J2	J3	J4	J5	J6	J7
Length distribution	count		56	175	677	453	31	117	77
	mean (m)		16,34	10,94	2,95	2,61	10,44	4,16	1,53
	std		12,31	8,78	2,10	1,41	6,27	2,93	0,80
	min (m)		1,42	0,11	0,09	0,37	3,26	0,29	0,52
	25th percentile (m)		7,33	4,19	1,43	1,57	7,54	2,29	0,97
	50th percentile (m)		13,31	7,89	2,41	2,26	9,37	3,36	1,22
	75th percentile (m)		21,96	14,46	3,88	3,35	11,44	4,77	1,69
	max (m)		53,04	42,90	17,39	9,34	36,20	17,38	4,16
	geom mean (m)		12,32	7,90	2,32	2,27	9,09	3,43	1,37
	CoV		0,75	0,80	0,71	0,54	0,59	0,70	0,52
	skewness		1,26	1,39	1,66	1,22	2,33	2,12	1,48
	kurtosis		1,00	1,56	4,49	1,84	7,35	5,07	1,62
Spacing	mean (m)		2,20	0,61	0,46	1,82	2,44	1,67	1,14
	median (m)		1,33	0,56	0,34	1,82	2,00	1,36	0,70
	variance		4,88	0,10	0,15	2,37	2,96	1,83	1,44
	geom mean (m)		1,51	0,54	0,34	1,30	1,92	1,26	0,78
		Area E	J1*		J4*	J5*	J6*		
Length distribution	count		362		682	119	236		
	mean (m)		10,47		2,77	3,82	3,26		
	std		7,88		1,35	2,72	2,26		
	min (m)		0,17		0,12	0,14	0,11		
	25th percentile (m)		4,76		1,77	1,97	1,66		
	50th percentile (m)		8,19		2,55	3,16	2,57		
	75th percentile (m)		14,50		3,50	5,20	3,93		
	max (m)		56,49		8,43	16,49	12,91		
	geom mean (m)		7,98		2,44	2,91	2,63		
	CoV		0,75		0,49	0,71	0,69		
	skewness		1,78		1,07	1,52	1,58		
	kurtosis		5,17		1,57	3,52	2,66		
Spacing	Mean		0,58		1,66	2,29	1,20		
	median		0,37		1,09	1,94	0,86		
	variance		0,29		2,95	1,71	0,95		
	geom mean		0,40		1,10	1,92	0,95		

717 **Table 2.** Length distribution and joint spacing per joint set and area.

718 **Supplementary Figures**



720 **Fig. S1.** Overview of the entire outcrop in a high detail image with all sets of mapped joints in Bench IV
721 highlighted: for clarity, only part of the joints present are outlined. In adjacent limestone layers, only mapped
722 joints of the oldest sets are shown.



724 **Fig. S2.** High resolution image of a small part of Area W with all existing joints of all sets mapped, including J8.
725 This is an enlargement of Figure 4f.